Neutrinoproduction of photons and pions from nucleons in a chiral effective field theory for nuclei

Brian D. Serot and Xilin Zhang*

Department of Physics and Center for Exploration of Energy and Matter, Indiana University, Bloomington, Indiana 47405, USA

(Received 31 March 2012; published 3 July 2012)

Neutrino-induced production (neutrinoproduction) of photons and pions from nucleons and nuclei is important for the interpretation of neutrino-oscillation experiments, as these photons and pions are potential backgrounds in the MiniBooNE experiment [A. A. Aquilar-Arevalo *et al*. (MiniBooNE Collaboration), Phys. Rev. Lett. **100**, 032301 (2008)]. These processes are studied at intermediate energies, where the $\Delta(1232)$ resonance becomes important. The Lorentz-covariant effective field theory, which is the framework used in this series of studies, contains nucleons, pions, Δs, isoscalar scalar (σ) and vector (ω) fields, and isovector vector (ρ) fields. The Lagrangian exhibits a nonlinear realization of (approximate) $\mathrm{SU}(2)_L \otimes \mathrm{SU}(2)_R$ chiral symmetry and incorporates vector meson dominance. In this paper, we focus on setting up the framework. Power counting for vertices and Feynman diagrams is explained. Because of the built-in symmetries, the vector current is automatically conserved, and the axial-vector current is partially conserved. To calibrate the axial-vector transition current ($N \leftrightarrow \Delta$), pion production from the nucleon is used as a benchmark and compared to bubble-chamber data from Argonne and Brookhaven National Laboratories. At low energies, the convergence of our power-counting scheme is investigated, and next-to-leading-order tree-level corrections are found to be small.

DOI: 10.1103/PhysRevC.86.015501 PACS number(s): 25.30.Pt, 11.30.Rd, 12.15.Ji, 24.10.Jv

I. INTRODUCTION

Neutrinoproduction of photons and pions from nucleons and nuclei plays an important role in the interpretation of neutrino-oscillation experiments, such as MiniBooNE [1]. The neutral current (NC) π^0 and photon production produce detector signals that resemble those of the desired $e^{\pm}$ signals. Currently, it is still a question whether NC photon production might explain the excess events seen at low reconstructed neutrino energies in the MiniBooNE experiment, which the MicroBooNE experiment plans to answer [2]. Moreover, pion absorption after production could lead to events that mimic quasielastic scattering.

Ultimately, the calculations must be done on nuclei, which are the primary detector materials in oscillation experiments. To separate the many-body effects from the reaction mechanism and to calibrate the elementary amplitude, we study charged current (CC) and NC pion production from free nucleons in this work, which serves as the benchmark. Moreover, NC photon production, which is not a topic under intense investigation, is studied within this calibrated framework. In future papers, we will include the electroweak response of the nuclear many-body system to discuss the productions from nuclei in the same framework.

Here we use a recently proposed Lorentz-covariant meson-baryon effective field theory (EFT) that was originally motivated by the nuclear many-body problem [3–10]. (This formalism is often called *quantum hadrodynamics* or QHD.) This QHD EFT includes all the relevant symmetries of the underlying QCD; in particular, the approximate, spontaneously broken $\mathrm{SU}(2)_L \otimes \mathrm{SU}(2)_R$ chiral symmetry is realized nonlinearly. The motivation for this EFT and some calculated results are discussed in Refs. [4,5,11–20]. In this EFT, we have the Δ resonance consistently incorporated as an explicit degree of freedom, while respecting the underlying symmetries of QCD noted earlier. (The generation of mesons and the Δ resonance through pion-pion interactions and pion-nucleon interactions has been investigated in [21,22].) We are concerned with the intermediate-energy region ($E_\nu^{\mathrm{Lab}} \leqslant 0.5$ GeV), where the resonant behavior of the Δ becomes important. The details about introducing Δ degree of freedom, the full Lagrangian, and electroweak interactions in this model have been presented in [23,24]. The well-known pathologies associated with introducing Δ are not relevant in the context of EFT. The couplings to electroweak fields are included using the external field technique [25], which allows us to deduce the electroweak currents. Because of the approximate symmetries in the Lagrangian, the vector currents are automatically conserved and the axial-vector currents are partially conserved. Form factors are generated within the theory by vector meson dominance (VMD), which allows us to avoid introducing phenomenological form factors and makes current conservation manifest.[1] We discuss the power counting of both vertices and diagrams on and off resonance and consistently keep all tree-level diagrams through next-to-leading order. Explicit power counting of loop diagrams in this EFT has been discussed in Refs. [17–19]. Here the contributions of the loops are assumed to be (mostly) saturated by heavy mesons and the Δ resonance, so the couplings of contact interactions are

*xilzhang@indiana.edu

[1]Meson dominance generates form factors for contact pion-production vertices automatically, as shown in diagram (f) in Fig. 1. In other approaches, for example [26], these form factors are introduced by hand, which requires specific relations between the nucleon vector current and the pion vector current form factors. This is explained in Secs. II B and IV.

viewed as being renormalized. The mesons' role in effective field theory has also been investigated in [27,28].

One major goal of this work is to calibrate electroweak interactions on the nucleon level. It is typically assumed that the vector part of the $N \to \Delta$ transition current is well constrained by electromagnetic interactions [29,30]. The uncertainty is in the axial-vector part of the current, which is determined by fitting to Argonne National Laboratory (ANL) [31] and Brookhaven National Laboratory (BNL) [32] bubble-chamber data. The data have large error bars, which leads to significant model dependence in the fitted results [26,33,34]. Here we choose one recently fitted parametrization [33] and use it to determine the constants of our VMD parametrization (but note that our basis of currents is different from the conventional one as used in [26,33,34]). In addition, we make use of other form factors, the ones in [26] for example. We then compare results of using different current basis and form factors with the data at low and intermediate neutrino energies.

There have been numerous earlier studies of neutrino-production of pions from nucleons in the resonance region [26,29,30,33,35–43]. They basically fall into two categories. In the first one [29,30,33,38,39,41] resonance dominance above intermediate energy is assumed. The contributions of resonances are summed incoherently and hence it is difficult to determine the interference effect. In the second category [26,35,40,42,43], the contributions are summed coherently including the background, since either an effective Hamiltonian or Lagrangian is utilized.

Our approach belongs to the second category, while differences from other models should be mentioned. First, there exists a finite energy range in which EFT is valid, so we insist on low-energy calculations. However, a different attitude has been taken, for example, in Refs. [26,42], in which the Born approximation based on an effective Lagrangian has been extrapolated to the region of several GeV. Second, we have discussed the consequence of higher-order contact terms.[2] Naturally, these contributions should obey naive power counting [44,45]; however, some of them may play an important role in scattering from nuclei. Third, electroweak interactions of nucleons are calibrated in this work while the strong interaction has been calibrated to nuclear properties. This is a unique feature that is absent in other models targeting the production from free nucleons only. Furthermore, the calibration on the nucleon's electroweak interaction impacts the strong interaction. For example, the $\rho\pi\pi$ coupling, introduced because of VMD in the pion's vector current, gives rise to an interesting contribution in the two-body axial current in a many-body calculation [46]. In our theory with Δ, it can be quite interesting to investigate similar consequences, for example, the Δ's role in the two-body current, in which meson-dominance couplings can give rise to relevant interactions.

This article is organized as follows: in Sec. II and III, we introduce our Lagrangian without and with Δ, and we calculate several current matrix elements that will be useful for the subsequent Feynman diagram calculations. The theory involving Δ is emphasized. Then the transition current basis and form factors are discussed carefully. In Sec. IV, we discuss our calculations for the CC and NC pion production and for the NC photon production. After that, we show our results in Sec. V. Whenever possible, we compare our results with available data and present our analysis. Finally, our conclusions are summarized in Sec. VI.

In the Appendixes, we present the necessary information about chiral symmetry and electroweak interactions in QHD EFT, form factor calculations, power counting for the diagram with Δ, and kinematics.

II. LAGRANGIAN WITHOUT $\Delta(1232)$

In this work, the metric $g_{\mu\nu} = \mathrm{diag}(1,-1,-1,-1)_{\mu\nu}$. The convention for the Levi-Civita symbol $\epsilon^{\mu\nu\alpha\beta}$ is $\epsilon^{0123} = 1$. We have introduced upper and lower isospin indices [23,24]. In this section, we focus on the Lagrangian without Δ and study various matrix elements: $\langle N|V^i_\mu, A^i_\mu, J^B_\mu|N\rangle$ and $\langle N;\pi|V^i_\mu, A^i_\mu, J^B_\mu|N\rangle$. Definitions of fields and currents can be found in Appendix A.

A. Power counting and the Lagrangian

The organization of interaction terms is based on power counting [5,17,18] and naive dimensional analysis (NDA) [44,45]. We associate with each interaction term an index $\hat{\nu} \equiv d + n/2 + b$. Here d is the number of derivatives (small momentum transfer) in the interaction, n is the number of fermion fields, and b is the number of heavy-meson fields. The Lagrangian is well developed in Refs. [10,23,24,47]. We begin with the Lagrangian

$$\begin{aligned}\mathcal{L}_{N(\hat{\nu}\leqslant 3)} = {}& \overline{N}(i\gamma^\mu[\widetilde{\partial}_\mu + ig_\rho\rho_\mu + ig_v V_\mu] \\ & + g_A\gamma^\mu\gamma^5\widetilde{a}_\mu - M + g_s\phi)N \\ & - \frac{f_\rho g_\rho}{4M}\overline{N}\rho_{\mu\nu}\sigma^{\mu\nu}N - \frac{f_v g_v}{4M}\overline{N}V_{\mu\nu}\sigma^{\mu\nu}N \\ & - \frac{\kappa_\pi}{M}\overline{N}\widetilde{v}_{\mu\nu}\sigma^{\mu\nu}N + \frac{4\beta_\pi}{M}\overline{N}N\,\mathrm{Tr}(\widetilde{a}_\mu\widetilde{a}^\mu) \\ & + \frac{1}{4M}\overline{N}\sigma^{\mu\nu}(2\lambda^{(0)}f_{s\mu\nu} + \lambda^{(1)}F^{(+)}_{\mu\nu})N \\ & + \frac{i\kappa_1}{2M^2}\overline{N}\gamma_\mu\overleftrightarrow{\widetilde{\partial}}_\nu N\,\mathrm{Tr}\,(\widetilde{a}^\mu\widetilde{a}^\nu)\,. \end{aligned} \tag{1}$$

$\widetilde{\partial}_\mu$ is defined in Eq. (A6), $\overleftrightarrow{\widetilde{\partial}}_\nu \equiv \widetilde{\partial}_\nu - (\overleftarrow{\partial}_\nu - i\widetilde{v}_\nu + iv_{(s)\nu})$, and the field tensors are $V_{\mu\nu} \equiv \partial_\mu V_\nu - \partial_\nu V_\mu$ and $\rho_{\mu\nu} \equiv \widetilde{\partial}_{[\mu}\rho_{\nu]} + i\overline{g}_\rho[\rho_\mu\,,\,\rho_\nu]$. The superscripts $^{(0)}$ and $^{(1)}$ denote the isospin. Next is a purely mesonic piece:

$$\begin{aligned}\mathcal{L}_{\mathrm{meson}(\hat{\nu}\leqslant 4)} = {}& \tfrac{1}{2}\,\partial_\mu\phi\,\partial^\mu\phi + \tfrac{1}{4}f_\pi^2\,\mathrm{Tr}[\widetilde{\partial}_\mu U(\widetilde{\partial}^\mu U)^\dagger] \\ & + \tfrac{1}{4}f_\pi^2 m_\pi^2\,\mathrm{Tr}(U + U^\dagger - 2) \\ & - \tfrac{1}{2}\,\mathrm{Tr}(\rho_{\mu\nu}\rho^{\mu\nu}) - \tfrac{1}{4}\,V^{\mu\nu}V_{\mu\nu} \\ & + \frac{1}{2g_\gamma}\big(\mathrm{Tr}(F^{(+)\mu\nu}\rho_{\mu\nu}) + \tfrac{1}{3}\,f_s^{\mu\nu}V_{\mu\nu}\big). \end{aligned} \tag{2}$$

We only show the kinematic terms and photon couplings to the vector fields. The latter are used to generate VMD. Other $\nu = 3$

[2] Some of these terms have also been discussed in Ref. [42]; however, the interpretation of these terms is different here from that in [42].

and $\nu = 4$ terms in $\mathcal{L}_{\text{meson}(\hat{\nu}\leqslant 4)}$ are important for describing the bulk properties of nuclear many-body systems and can be found in [5,23,24,48,49]. The only manifest chiral-symmetry breaking is through the nonzero pion mass. Other chiral-symmetry-violating terms and multiple pion interactions are not considered in this calculation. Finally, we have

$$\begin{aligned}\mathcal{L}_{N,\pi(\hat{\nu}=4)} = {} & \frac{1}{2M^2}\,\overline{N}\gamma_\mu\big(2\beta^{(0)}\partial_\nu f_s^{\mu\nu} + \beta^{(1)}\widetilde{\partial}_\nu F^{(+)\mu\nu} + \beta_A^{(1)}\gamma^5\widetilde{\partial}_\nu F^{(-)\mu\nu}\big)N - \omega_1\,\mathrm{Tr}(F_{\mu\nu}^{(+)}\widetilde{v}^{\mu\nu}) + \omega_2\,\mathrm{Tr}(\widetilde{a}_\mu\widetilde{\partial}_\nu F^{(-)\mu\nu}) \\ & + \omega_3\,\mathrm{Tr}(\widetilde{a}_\mu i[\widetilde{a}_\nu,\ F^{(+)\mu\nu}]) - g_{\rho\pi\pi}\frac{2f_\pi^2}{m_\rho^2}\,\mathrm{Tr}(\rho_{\mu\nu}\widetilde{v}^{\mu\nu}) + \frac{c_1}{M^2}\,\overline{N}\gamma^\mu N\,\mathrm{Tr}(\widetilde{a}^\nu\,\overline{F}_{\mu\nu}^{(+)}) \\ & + \frac{e_1}{M^2}\,\overline{N}\gamma^\mu\,\widetilde{a}^\nu N\,\overline{f}_{s\mu\nu} + \frac{c_{1\rho}g_\rho}{M^2}\,\overline{N}\gamma^\mu N\,\mathrm{Tr}(\widetilde{a}^\nu\,\overline{\rho}_{\mu\nu}) + \frac{e_{1v}g_v}{M^2}\,\overline{N}\gamma^\mu\,\widetilde{a}^\nu N\,\overline{V}_{\mu\nu}. \end{aligned} \tag{3}$$

Note that $\mathcal{L}_{N,\pi(\hat{\nu}=4)}$ is not a complete list of all possible $\hat{\nu} = 4$ interaction terms. The terms listed in the first two rows generate the form factors of currents for nucleons and pions. $g_{\rho\pi\pi}$ is used for VMD. Special attention should be given to the c_1, e_1, $c_{1\rho}$, and $e_{1\rho}$ couplings, since they are the only relevant $\hat{\nu} = 4$ terms for NC photon production. Further discussion will be given in Secs. IV C and V D.

B. Contributions to current matrix elements from irreducible diagrams

To calculate various current matrix elements, we need to understand the background fields in terms of electroweak boson fields; this connection is given in Appendix A. Based on the Lagrangian, we can calculate the matrix elements $\langle N|V_\mu^i,\ A_\mu^i,\ J_\mu^B|N\rangle$ and $\langle N;\pi|V_\mu^i,\ A_\mu^i,\ J_\mu^B|N\rangle$ [diagram (f) in Fig. 1] at tree level; loops are not included; only diagrams with contact structure are included.[3] Because of VMD, we can extrapolate the current to nonzero Q^2 [10,20]. The results are given below, and the explicit calculations are shown in Appendix A. Note that q^μ is defined as the *incoming* momentum transfer at the vertex; in terms of initial and final nucleon momenta, $q^\mu \equiv p_{nf}^\mu - p_{ni}^\mu$. Similarly, $q^\mu + p_{ni}^\mu = p_{nf}^\mu + k_\pi^\mu$ for pion production.

First, the matrix elements of the nucleon's vector and baryon current and the axial-vector current in pion production are the following:

$$\langle N,B|V_\mu^i|N,A\rangle = \langle B|\frac{\tau^i}{2}|A\rangle\,\overline{u}_f\left(\gamma_\mu + 2\delta F_1^{V,md}\,\frac{q^2\gamma_\mu - \not{q}q_\mu}{q^2} + 2F_2^{V,md}\,\frac{\sigma_{\mu\nu}iq^\nu}{2M}\right)u_i \equiv \langle B|\frac{\tau^i}{2}|A\rangle\,\overline{u}_f\Gamma_{V\mu}(q)u_i, \tag{4}$$

$$\langle N,B|J_\mu^B|N,A\rangle = \delta_B^A\,\overline{u}_f\left(\gamma_\mu + 2\delta F_1^{S,md}\,\frac{q^2\gamma_\mu - \not{q}q_\mu}{q^2} + 2F_2^{S,md}\frac{\sigma_{\mu\nu}iq^\nu}{2M}\right)u_i \equiv \delta_B^A\,\overline{u}_f\Gamma_{B\mu}(q)u_i, \tag{5}$$

$$\begin{aligned}\langle N,B;\pi,j,k_\pi|A_\mu^i|N,A\rangle = {} & -\frac{\epsilon_{jk}^i}{f_\pi}\,\langle B|\frac{\tau^k}{2}|A\rangle\,\overline{u}_f\gamma^\nu u_i\left[g_{\mu\nu} + 2\delta F_1^{V,md}((q-k_\pi)^2)\frac{q\cdot(q-k_\pi)g_{\mu\nu} - (q-k_\pi)_\mu q_\nu}{(q-k_\pi)^2}\right] \\ & - \frac{\epsilon_{jk}^i}{f_\pi}\,\langle B|\frac{\tau^k}{2}|A\rangle\,\overline{u}_f\frac{\sigma_{\mu\nu}iq^\nu}{2M}\,u_i\left[2\lambda^{(1)} + 2\delta F_2^{V,md}((q-k_\pi)^2)\,\frac{q\cdot(q-k_\pi)}{(q-k_\pi)^2}\right] \\ \equiv {} & \frac{\epsilon_{jk}^i}{f_\pi}\,\langle B|\frac{\tau^k}{2}|A\rangle\,\overline{u}_f\Gamma_{A\pi\mu}(q,k_\pi)u_i. \end{aligned} \tag{6}$$

Here $m_\rho = 0.776$ GeV, $m_v = 0.783$ GeV, $\delta F \equiv F(q^2) - F(0)$ (also true for other form factors), and

$$F_1^{V,md} = \frac{1}{2}\left(1 + \frac{\beta^{(1)}}{M^2}\,q^2 - \frac{g_\rho}{g_\gamma}\frac{q^2}{q^2-m_\rho^2}\right),\ \beta^{(1)} = -1.35,\ \frac{g_\rho}{g_\gamma} = 2.48, \tag{7}$$

$$F_2^{V,md} = \frac{1}{2}\left(2\lambda^{(1)} - \frac{f_\rho g_\rho}{g_\gamma}\frac{q^2}{q^2-m_\rho^2}\right),\ \lambda^{(1)} = 1.85,\ f_\rho = 3.04, \tag{8}$$

$$F_1^{S,md} = \frac{1}{2}\left(1 + \frac{\beta^{(0)}}{M^2}\,q^2 - \frac{2g_v}{3g_\gamma}\frac{q^2}{q^2-m_v^2}\right),\quad \beta^{(0)} = -1.40,\ \frac{g_v}{g_\gamma} = 3.95, \tag{9}$$

$$F_2^{S,md} = \frac{1}{2}\left(2\lambda^{(0)} - \frac{2f_v g_v}{3g_\gamma}\frac{q^2}{q^2-m_v^2}\right),\ \lambda^{(0)} = -0.06,\ f_v = -0.19. \tag{10}$$

[3]The expressions for the currents listed below differ from those in Refs. [10,46] because contributions from nonminimal and vector-meson-dominance terms are included here.

We can also use this procedure to expand the axial-vector current in powers of q^2 using the Lagrangian constants g_A and $\beta_A^{(1)}$. In fact, we can improve on this by including the axial-vector meson ($a_{1\mu}$) contribution to the matrix elements, which would arise from the interactions $g_{a_1}\overline{N}\gamma^\mu\gamma^5 a_{1\underline{\mu}}N$ and $c_{a_1}\,\mathrm{Tr}\left(F^{(-)\mu\nu}a_{1\mu\nu}\right)$. Here $a_{1\mu}=a_{1i\mu}\tau^i/2$ and $a_{1\mu\nu}\equiv\widetilde{\partial}_\mu a_{1\nu}-\widetilde{\partial}_\nu a_{1\mu}$, where $a_{1i\mu}$ are the fields of the a_1 meson (with its mass denoted as $m_{a_1}=1.26$ GeV). Then we obtain

$$\langle N,B|A^i_\mu|N,A\rangle=-G_A^{md}(q^2)\,\langle B|\frac{\tau^i}{2}|A\rangle\,\overline{u}_f\left(\gamma_\mu-\frac{q_\mu\,\not{q}}{q^2-m_\pi^2}\right)\gamma^5 u_i\equiv\langle B|\frac{\tau^i}{2}|A\rangle\,\overline{u}_f\Gamma_{A\mu}(q)u_i, \tag{11}$$

$$\begin{aligned}\langle N,B,\pi,j|V^i_\mu|N,A\rangle&=\frac{\epsilon^i_{jk}}{f_\pi}\,\langle B|\frac{\tau^k}{2}|A\rangle\,\overline{u}_f\left(G_A^{md}(0)\gamma_\mu\gamma^5+\delta G_A^{md}((q-k_\pi)^2)\,\frac{q\cdot(q-k_\pi)g_{\mu\nu}-(q-k_\pi)_\mu q_\nu}{(q-k_\pi)^2}\,\gamma^\nu\gamma^5\right)u_i\\&\equiv\frac{\epsilon^i_{jk}}{f_\pi}\,\langle B|\frac{\tau^k}{2}|A\rangle\,\overline{u}_f\Gamma_{V\pi\mu}(q,k_\pi)u_i,\end{aligned} \tag{12}$$

$$G_A^{md}(q^2)\equiv g_A-\beta_A^{(1)}\,\frac{q^2}{M^2}-\frac{2c_{a_1}g_{a_1}q^2}{q^2-m_{a_1}^2},\ g_A=1.26,\ \beta_A^{(1)}=2.27,\ c_{a_1}g_{a_1}=3.85. \tag{13}$$

For the pion's vector current form factor [5],

$$\begin{aligned}\langle\pi,k,k_\pi|V^i_\mu|\pi,j,k_\pi-q\rangle&=i\epsilon^{ij}{}_k\left[(2k_\pi-q)_\mu+2\delta F_\pi^{md}(q^2)\left(k_{\pi\mu}-\frac{q\cdot k_\pi}{q^2}\,q_\mu\right)\right]\equiv i\epsilon^{ij}{}_k\,P_{V\mu}(q,k_\pi),\\F_\pi^{md}(q^2)&\equiv\left(1-\frac{g_{\rho\pi\pi}}{g_\gamma}\,\frac{q^2}{q^2-m_\rho^2}\right),\quad\frac{g_{\rho\pi\pi}}{g_\gamma}=1.20.\end{aligned} \tag{14}$$

To determine the couplings in Eqs. (7), (8), (9), (10), (13), and (14), we compare our results with the fitted form factors [5,50]. We require that the behavior of our vector- and baryon-meson-dominance form factors near $Q^2=0$ be close to that of the fitted form factors [50]. The nucleon's axial-vector current used to fit our G_A^{md} is parametrized as $G_A(q^2)=g_A/(1-q^2/M_A^2)^2$ with $g_A=1.26$ and $M_A=1.05$ GeV [51]. As shown in Ref. [20], the form factors due to vector meson dominance become inadequate at $Q^2\approx 0.3$ GeV^2. This is also true for the axial vector's parametrization. This indicates that the EFT Lagrangian is only applicable for $E_l\leqslant 0.5$ GeV in lepton–nucleon interactions, above which Q^2 exceeds the limit. This will be clarified in the kinematical analysis of Sec. V A.

III. LAGRANGIAN INVOLVING Δ(1232)

A. Lagrangian

Two remarks are in order here [23,24]: First, the theory is self-consistent with general interactions involving ψ^μ; second, the so-called off-shell couplings, which have the form $\gamma_\mu\psi^\mu$, $\widetilde{\partial}_\mu\psi^\mu$, $\overline{\psi}^\mu\gamma_\mu$, and $\widetilde{\partial}_\mu\overline{\psi}^\mu$, can be considered as redundant. For the chiral symmetry realization, Δ^{*a} belong to an $I=3/2$ multiplet [$a=(\pm3/2,\pm1/2)$]. Moreover, in the power counting of vertices, the Δ is counted in the same way as nucleons.

Consider first $\mathcal{L}_\Delta$ ($\hat{\nu}\leqslant 3$):

$$\begin{aligned}\mathcal{L}_\Delta=&\frac{-i}{2}\,\overline{\Delta}^a_\mu\{\sigma^{\mu\nu},\,(i\,\widetilde{\not\partial}-h_\rho\,\not\rho-h_v\,\not V-m+h_s\phi)\}^b_a\,\Delta_{b\nu}\\&+\widetilde{h}_A\overline{\Delta}^a_\mu\,\widetilde{\not a}^b_a\gamma^5\Delta^\mu_b\\&-\frac{\widetilde{f}_\rho h_\rho}{4m}\,\overline{\Delta}_\lambda\,\rho_{\mu\nu}\sigma^{\mu\nu}\Delta^\lambda-\frac{\widetilde{f}_v h_v}{4m}\,\overline{\Delta}_\lambda V_{\mu\nu}\sigma^{\mu\nu}\Delta^\lambda\\&-\frac{\widetilde{\kappa}_\pi}{m}\,\overline{\Delta}_\lambda\widetilde{v}_{\mu\nu}\sigma^{\mu\nu}\Delta^\lambda+\frac{4\widetilde{\beta}_\pi}{m}\,\overline{\Delta}_\lambda\Delta^\lambda\,\mathrm{Tr}(\widetilde{a}^\mu\,\widetilde{a}_\mu).\end{aligned} \tag{15}$$

This is essentially a copy of the corresponding Lagrangian for nucleons.

To produce the $N\leftrightarrow\Delta$ transition currents, we construct the following Lagrangians ($\hat{\nu}\leqslant 4$):

$$\mathcal{L}_{\Delta,N,\pi}=h_A\overline{\Delta}^{a\mu}\,T^{\dagger iA}_a\,\widetilde{a}_{i\mu}N_A+\mathrm{c.c.}, \tag{16}$$

$$\begin{aligned}\mathcal{L}_{\Delta,N,\mathrm{bg}}=&\frac{ic_{1\Delta}}{M}\,\overline{\Delta}^a_\mu\gamma_\nu\gamma^5\,T^{\dagger iA}_a F_i^{(+)\mu\nu}N_A+\frac{ic_{3\Delta}}{M^2}\,\overline{\Delta}^a_\mu\,i\gamma^5\,T^{\dagger iA}_a(\widetilde{\partial}_\nu F^{(+)\mu\nu})_i N_A+\frac{c_{6\Delta}}{M^2}\,\overline{\Delta}^a_\lambda\sigma_{\mu\nu}T^{\dagger iA}_a(\widetilde{\partial}^\lambda\overline{F}^{(+)\mu\nu})_i N_A\\&-\frac{d_{2\Delta}}{M^2}\,\overline{\Delta}^a_\mu\,T^{\dagger iA}_a(\widetilde{\partial}_\nu F^{(-)\mu\nu})_i N_A-\frac{id_{4\Delta}}{M}\,\overline{\Delta}^a_\mu\gamma_\nu\,T^{\dagger iA}_a F_i^{(-)\mu\nu}N_A-\frac{id_{7\Delta}}{M^2}\,\overline{\Delta}^a_\lambda\sigma_{\mu\nu}T^{\dagger iA}_a(\widetilde{\partial}^\lambda F^{(-)\mu\nu})_i N_A+\mathrm{c.c.},\end{aligned} \tag{17}$$

$$\mathcal{L}_{\Delta,N,\rho}=\frac{ic_{1\Delta\rho}}{M}\,\overline{\Delta}^a_\mu\,\gamma_\nu\gamma^5\,T^{\dagger iA}_a\rho_i^{\mu\nu}N_A+\frac{ic_{3\Delta\rho}}{M^2}\,\overline{\Delta}^a_\mu\,i\gamma^5\,T^{\dagger iA}_a(\widetilde{\partial}_\nu\rho^{\mu\nu})_i N_A+\frac{c_{6\Delta\rho}}{M^2}\,\overline{\Delta}^a_\lambda\sigma_{\mu\nu}\,T^{\dagger iA}_a(\widetilde{\partial}^\lambda\,\overline{\rho}^{\mu\nu})_i N_A+\mathrm{c.c.}. \tag{18}$$

Here $T_a^{\dagger\, iA} = \langle \frac{3}{2}; a | 1, \frac{1}{2}; i, A \rangle$, which are (complex conjugate of) Clebsch-Gordan coefficients.

B. Transition currents

We can express the transition current's matrix element as follows:

$$\langle \Delta, a, p_\Delta | V^{i\mu}(A^{i\mu}) | N, A, p_N \rangle \equiv T_a^{\dagger\, iA}\, \overline{u}_{\Delta\alpha}(p_\Delta)\, \Gamma^{\alpha\mu}_{V(A)}(q)\, u_N(p_N). \tag{19}$$

Based on the Lagrangians, we find (noting that $\sigma_{\mu\nu}\epsilon^{\mu\nu\alpha\beta} \propto i\sigma^{\alpha\beta}\gamma^5$)

$$\begin{aligned}\Gamma_V^{\alpha\mu} &= \frac{2c_{1\Delta}(q^2)}{M}(q^\alpha\gamma^\mu - \not{q} g^{\alpha\mu})\gamma^5 \\ &\quad + \frac{2c_{3\Delta}(q^2)}{M^2}(q^\alpha q^\mu - g^{\alpha\mu}q^2)\gamma^5 \\ &\quad - \frac{8c_{6\Delta}(q^2)}{M^2} q^\alpha \sigma^{\mu\nu} i q_\nu \gamma^5,\end{aligned} \tag{20}$$

$$\begin{aligned}\Gamma_A^{\alpha\mu} &= -h_A\left(g^{\alpha\mu} - \frac{q^\alpha q^\mu}{q^2 - m_\pi^2}\right) \\ &\quad + \frac{2d_{2\Delta}}{M^2}(q^\alpha q^\mu - g^{\alpha\mu}q^2) \\ &\quad - \frac{2d_{4\Delta}}{M}(q^\alpha\gamma^\mu - g^{\alpha\mu}\not{q}) - \frac{4d_{7\Delta}}{M^2} q^\alpha \sigma^{\mu\nu} i q_\nu,\end{aligned} \tag{21}$$

$$\begin{aligned}c_{i\Delta}(q^2) &\equiv c_{i\Delta} + \frac{c_{i\Delta\rho}}{2g_\gamma}\frac{q^2}{q^2 - m_\rho^2}, \quad i = 1, 3, 6, \\ c_{1\Delta} &= 1.21, \quad c_{3\Delta} = -0.61, \quad c_{6\Delta} = -0.078, \\ \frac{c_{1\Delta\rho}}{g_\gamma} &= -4.58, \quad \frac{c_{3\Delta\rho}}{g_\gamma} = 2.32, \quad \frac{c_{6\Delta\rho}}{g_\gamma} = 0.30.\end{aligned} \tag{22}$$

Similar to the $c_{i\Delta}(q^2)$, we can introduce axial-vector meson exchange into the axial transition current, which leads to a structure for the $d_{i\Delta}(q^2)$ similar to that of the $c_{i\Delta}(q^2)$. There is one subtlety associated with the realization of $h_A(q^2)$: with our Lagrangian, we have a pion-pole contribution associated with the h_A coupling, and all the higher-order terms contained in $\delta h_A(q^2) \equiv h_A(q^2) - h_A$ conserve the axial transition current. With the limited information about manifest chiral-symmetry breaking, we ignore this subtlety and still use the form of the $c_{1\Delta}(q^2)$ to parametrize $h_A(q^2)$:

$$\begin{aligned}h_A(q^2) &\equiv h_A + h_{\Delta a_1}\frac{q^2}{q^2 - m_{a_1}^2}, \\ h_A &= 1.40, \quad h_{\Delta a_1} = -3.98,\end{aligned} \tag{23}$$

$$\begin{aligned}d_{i\Delta}(q^2) &\equiv d_{i\Delta} + d_{i\Delta a_1}\frac{q^2}{q^2 - m_{a_1}^2}, \quad i = 2, 4, 7, \\ d_{2\Delta} &= -0.087, \quad d_{4\Delta} = 0.20, \quad d_{7\Delta} = -0.04, \\ d_{2\Delta a_1} &= 0.25, \quad d_{4\Delta a_1} = -0.58, \quad d_{7\Delta a_1} = 0.12.\end{aligned} \tag{24}$$

To determine the coefficients in the transition form factors shown in Eqs. (22), (23), and (24), we compare ours with one of the conventional form factors used in the literature. In Refs. [26,33] for example, the definition for $\langle \Delta, \frac{1}{2} | j^\mu_{cc+} | N, -\frac{1}{2} \rangle$ [$= -\sqrt{2/3}\, \overline{u}_\alpha(p_\Delta)\left(\Gamma_V^{\alpha\mu} + \Gamma_A^{\alpha\mu}\right) u(p_N)$] is

$$\begin{aligned}&\overline{u}_\alpha(p_\Delta)\left\{\left[\frac{C_3^V}{M}(g^{\alpha\mu}\not{q} - q^\alpha\gamma^\mu) + \frac{C_4^V}{M^2}(q\cdot p_\Delta\, g^{\alpha\mu} - q^\alpha p_\Delta^\mu) + \frac{C_5^V}{M^2}\left(q\cdot p_N\, g^{\alpha\mu} - q^\alpha p_N^\mu\right)\right]\gamma^5\right. \\ &\quad \left. + \left[\frac{C_3^A}{M}(g^{\alpha\mu}\not{q} - q^\alpha\gamma^\mu) + \frac{C_4^A}{M^2}(q\cdot p_\Delta\, g^{\alpha\mu} - q^\alpha p_\Delta^\mu) + C_5^A g^{\alpha\mu} + \frac{C_6^A}{M^2} q^\mu q^\alpha\right]\right\} u(p_N).\end{aligned} \tag{25}$$

We use the "Adler parametrization" [35] in Ref. [33] to fit our meson-dominance form factors. Now supposing the baryons are on shell, we can represent the conventional basis as linear combinations of our basis. For example,

$$\begin{aligned}q^\alpha\sigma^{\mu\nu} i q_\nu \gamma^5 &= (m - M)(q^\alpha\gamma^\mu - g^{\alpha\mu}\not{q})\gamma^5 \\ &\quad - (q^\alpha p_\Delta^\mu - q\cdot p_\Delta g^{\alpha\mu})\gamma^5 \\ &\quad - (q^\alpha p_N^\mu - q\cdot p_N g^{\alpha\mu})\gamma^5.\end{aligned} \tag{26}$$

A similar relation holds with γ^5 deleted on both sides and $(m - M)$ changed to $(m + M)$. We can obtain the relation between form factors associated with the two bases:

$$c_{1\Delta} = \sqrt{\frac{3}{2}}\left[\frac{C_3^V}{2} + \frac{m - M}{2M}\frac{\left(C_4^V + C_5^V\right)}{2}\right], \tag{27}$$

$$c_{3\Delta} = \sqrt{\frac{3}{2}}\frac{\left(C_4^V - C_5^V\right)}{4}, \quad c_{6\Delta} = \sqrt{\frac{3}{2}}\frac{\left(C_4^V + C_5^V\right)}{16}, \tag{28}$$

$$h_A = \sqrt{\frac{3}{2}}\, C_5^A, \quad d_{2\Delta} = \sqrt{\frac{3}{2}}\,\frac{C_4^A}{4}, \tag{29}$$

$$d_{4\Delta} = -\sqrt{\frac{3}{2}}\left(\frac{C_3^A}{2} + \frac{m + M}{2M}\frac{C_4^A}{2}\right), \quad d_{7\Delta} = \sqrt{\frac{3}{2}}\,\frac{C_4^A}{8}. \tag{30}$$

We assume that these relations hold away from the resonance. It can be shown that, at low energy, the differences in observables due to using the two bases, with these relations applied, are negligible. Moreover, the q^2 dependence of these $c_{i\Delta}$ and $d_{i\Delta}$ form factors can be realized in terms of meson dominance. We then require that the meson-dominance form factors be as close as possible to the ones indicated in Eqs. (27) to (30), and we get the couplings shown in Eqs. (22), (23), and (24). However, we should expect the leading-order meson-dominance expressions would fail above $Q^2 \approx 0.3\ \mathrm{GeV}^2$.

IV. FEYNMAN DIAGRAMS

Tree-level Feynman diagrams for pion production due to the vector current, axial-vector current, and baryon current are shown in Fig. 1. In this section, we calculate different matrix elements for pion production and photon production. The Feynman diagrams for photon production can be viewed as diagrams in Fig. 1 with an outgoing π line changed to a γ line. It turns out that diagram (e) in Fig. 1 is negligible in NC photon production, since it is associated with $1-4\sin^2\theta_w$ [42].

First let us outline the calculation of the interaction amplitude M. Consider CC pion production (in the one-weak-boson-exchange approximation):

$$M = 4\sqrt{2}\,G_F V_{ud}\left\langle J^{(\mathrm{lep})}_{Li\mu}\right\rangle\left\langle J^{(\mathrm{had})i\mu}_{L}\right\rangle_\pi, \tag{31}$$

where $i=+1,-1$. In Eq. (31), G_F is the Fermi constant, V_{ud} is the CKM matrix element corresponding to u and d quark mixing, and $\langle J^{(\mathrm{had})i\mu}_L\rangle_\pi \equiv \langle NB,\pi j|J^{i\mu}_L|NA\rangle$. (The definitions of currents can be found in Appendix A.) $\langle J^{(\mathrm{lep})}_{Li\mu}\rangle \equiv \langle l(\bar{l})|J_{Li\mu}|\nu_l(\bar{\nu}_l)\rangle$ is the well-known leptonic-charged-current matrix element. For NC pion production, we need to set $V_{ud}=1$, $\langle J^{(\mathrm{had})i\mu}_L\rangle_\pi \to \langle J^{(\mathrm{had})\mu}_{NC}\rangle_\pi$, and $\langle J^{(\mathrm{lep})}_{Li\mu}\rangle \to \langle J^{(\mathrm{lep})}_{NC\mu}\rangle$ in Eq. (31). Here $\langle J^{(\mathrm{lep})}_{NC\mu}\rangle$ is the leptonic-neutral-current matrix element, and $\langle J^{(\mathrm{had})\mu}_{NC}\rangle_\pi \equiv \langle NB,\pi j|J^{\mu}_{NC}|NA\rangle$. For NC photon production, we have an expression similar to that of NC pion production with $\langle J^{(\mathrm{had})\mu}_{NC}\rangle_\pi \to \langle J^{(\mathrm{had})\mu}_{NC}\rangle_\gamma$, while $\langle J^{(\mathrm{had})\mu}_{NC}\rangle_\gamma \equiv \langle NB,\gamma|J^{\mu}_{NC}|NA\rangle$.

Now consider the power counting for $\langle J^{(\mathrm{had})\mu}\rangle_{\pi(\gamma)}$ in Eq. (31) for various processes. The order of the diagram (ν) is counted as [47] $\nu = 2L+2-E_n/2+\sum_i \#_i(\hat{\nu}_i-2)$, where L is the number of loops, E_n is the number of external baryon lines, $\hat{\nu}_i \equiv d_i + n_i/2 + b_i$ is the order of the vertex ($\hat{\nu}$) mentioned in Sec. II A, and $\#_i$ is the number of times that particular vertex appears. However, there is a subtlety related with power counting of diagrams with Δ, which has been carefully discussed in Ref. [52]. Compared to the normal power counting mentioned above, in which the baryon propagator scales as $1/O(Q)$, for diagrams involving one Δ in the s channel, we take $\nu \to \nu-1$ in the resonance regime and $\nu \to \nu+1$ away from the resonance. Details can be found in Appendix C.

Finally, conservation of vector current, conservation of baryon current, and partial conservation of axial-vector current can be easily checked for the matrix elements shown in the following.

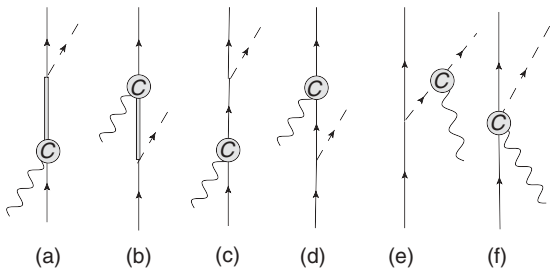

FIG. 1. Feynman diagrams for pion production. Here, **C** stands for various types of currents including vector, axial-vector, and baryon currents. Some diagrams may be zero for some specific type of current. For example, diagrams (a) and (b) will not contribute for the (isoscalar) baryon current. Diagram (e) will be zero for the axial-vector current. The pion-pole contributions to the axial current in diagrams (a), (b), (c), (d), and (f) are included in the vertex functions of the currents.

A. Diagram (a) and (b)

Diagram (a) and (b) in Fig. 1 lead to currents

$$\begin{aligned}\langle V^{i\mu}(A^{i\mu})\rangle_\pi &= -\frac{ih_A}{f_\pi}\,T^a_{Bj}\,T^{\dagger\,iA}_{a}\,\overline{u}_f k^\lambda_\pi\,S_{F\lambda\alpha}(p)\,\Gamma^{\alpha\mu}_{V(A)}(p;q,p_i)u_i \\ &\quad -\frac{ih_A}{f_\pi}\,T^{ai}_{B}\,T^{\dagger\,A}_{ja}\,\overline{u}_f\overline{\Gamma}^{\mu\alpha}_{V(A)}(p_f;q,p)S_{F\alpha\lambda}(p)\,k^\lambda_\pi\,u_i,\end{aligned} \tag{32}$$

where k_π is the outgoing pion's momentum. $\Gamma^{\alpha\mu}_{V(A)}(p;q,p_i)$ are defined in Eq. (19) while Δ's momentum is $p=q+p_i$. $\overline{\Gamma}^{\mu\alpha}_{V(A)}(p_f;q,p)\equiv\gamma^0\Gamma^{\dagger\alpha\mu}_{V(A)}(p;-q,p_f)\gamma^0$ while $p=-q+p_f$. In the following, we always have this definition of $\overline{\Gamma}$. The Δ's propagator, $S_{F\mu\nu}(p)$, is shown in Appendix D. The subscript j denotes the isospin of the outgoing pion. For vector current, in diagram (a) $\nu_{nr}\geqslant 3$ in the lower-energy region and $\nu_r\geqslant 1$ in the resonance region; in diagram (b) $\nu_{nr}\geqslant 3$. For axial-vector current, in diagram (a) $\nu_{nr}\geqslant 2$, $\nu_r\geqslant 0$; in diagram (b) $\nu_{nr}\geqslant 2$. In the power counting, the higher-order terms in ν come from including form factors at the vertices. Moreover, the baryon current matrix element is zero ($\langle J^\mu_B\rangle_\pi = 0$) in both diagrams.

Now we examine the NC matrix element $\langle J^{(\mathrm{had})\mu}_{NC}\rangle_\gamma$. First, based on the relations given in Eq. (A18), we define

$$\begin{aligned}\Gamma^{\alpha\mu}_N(p;q,p_i) &\equiv \left(\tfrac{1}{2}-\sin^2\theta_w\right)\Gamma^{\alpha\mu}_V(p;q,p_i) \\ &\quad +\tfrac{1}{2}\,\Gamma^{\alpha\mu}_A(p;q,p_i),\end{aligned} \tag{33}$$

Then we find

$$\begin{aligned}\left\langle J^\mu_{NC}\right\rangle_\gamma &= eT^a_{0B}\,T^{\dagger\,0A}_{a}\,\overline{u}_f\,\epsilon^*_\lambda(k)\overline{\Gamma}^{\lambda\alpha}_V(p_f;-k,p) \\ &\quad\times S_{F\alpha\beta}(p)\Gamma^{\beta\mu}_N(p;q,p_i)u_i \\ &\quad + eT^{a0}_{B}\,T^{\dagger\,A}_{a0}\,\overline{u}_f\overline{\Gamma}^{\mu\alpha}_N(p_f;q,p) \\ &\quad\times S_{F\alpha\beta}(p)\Gamma^{\beta\lambda}_V(p;-k,p_i)\,\epsilon^*_\lambda(k)\,u_i,\end{aligned} \tag{34}$$

where k is the outgoing photon's momentum and $\epsilon^*_\lambda(k)$ is its polarization. For the vector current in the NC, in diagram (a) $\nu_{nr}\geqslant 4$, $\nu_r\geqslant 2$; in diagram (b) $\nu_{nr}\geqslant 4$. For the axial-vector current, in diagram (a) $\nu_{nr}\geqslant 3$, $\nu_r\geqslant 1$; in diagram (b) $\nu_{nr}\geqslant 3$.

B. Diagrams (c) and (d)

These two diagrams lead to currents

$$\begin{aligned}\langle V^{i\mu}(A^{i\mu})\rangle_\pi &= -\frac{ig_A}{f_\pi}\,\langle B|\frac{\tau_j}{2}\frac{\tau^i}{2}|A\rangle\,\overline{u}_f\,\not{k}_\pi\gamma^5 S_F(p)\Gamma^\mu_{V(A)}(q)u_i \\ &\quad -\frac{ig_A}{f_\pi}\,\langle B|\frac{\tau^i}{2}\frac{\tau_j}{2}|A\rangle\,\overline{u}_f\Gamma^\mu_{V(A)}(q)S_F(p)\,\not{k}_\pi\gamma^5 u_i.\end{aligned} \tag{35}$$

For the nucleon propagator, $p = q + p_i$ in diagram (c) and $p = -q + p_f$ in diagram (d). $\Gamma^\mu_{V(A)}(q)$ has been defined in Eq. (4). For both currents in both diagrams $\nu \geqslant 1$. For the baryon current we just need to change $\frac{\tau^i}{2}\Gamma^\mu_V(q)$ to $\Gamma^\mu_B(q)$ in Eq. (35), and $\nu \geqslant 1$.

For NC photon production, we get

$$\begin{aligned}\left\langle J^\mu_{NC}\right\rangle_\gamma &= e\,\overline{u}_f\,\epsilon^*_\lambda(k)\left(\left(\frac{\tau^0}{2}\right)^C_B\Gamma^\lambda_V(-k)+\frac{\delta^C_B}{2}\Gamma^\lambda_B(-k)\right)S_F(p)\\ &\times\left(\left(\frac{\tau^0}{2}\right)^A_C\left[\left(\frac{1}{2}-\sin^2\theta_w\right)\Gamma^\mu_V(q)+\frac{1}{2}\Gamma^\mu_A(q)\right]-\frac{\delta^A_C}{2}\sin^2\theta_w\,\Gamma^\mu_B(q)\right)u_i\\ &+e\,\overline{u}_f\left(\left(\frac{\tau^0}{2}\right)^C_B\left[\left(\frac{1}{2}-\sin^2\theta_w\right)\Gamma^\mu_V(q)+\frac{1}{2}\Gamma^\mu_A(q)\right]-\frac{\delta^C_B}{2}\sin^2\theta_w\Gamma^\mu_B(q)\right)\\ &\times S_F(p)\,\epsilon^*_\lambda(k)\left(\left(\frac{\tau^0}{2}\right)^A_C\Gamma^\lambda_V(-k)+\frac{\delta^A_C}{2}\Gamma^\lambda_B(-k)\right)u_i,\end{aligned}\tag{36}$$

where we use the shorthand $(\frac{\tau^0}{2})^A_B = \langle B|\frac{\tau^0}{2}|A\rangle$. For all three currents, power counting gives $\nu \geqslant 1$. However, this naive power counting does not give an accurate comparison between the Δ contributions and the N contributions at low energies, as we discuss later.

C. Diagrams (e) and (f)

The two diagrams lead to a vector current

$$\langle V^{i\mu}\rangle_\pi = \frac{g_A}{f_\pi}\,\epsilon^i{}_{jk}\langle B|\frac{\tau^k}{2}|A\rangle\,\frac{P^\mu_V(q,k_\pi)}{(q-k_\pi)^2-m_\pi^2}\,\overline{u}_f(\not{q}-\not{k}_\pi)\gamma^5\,u_i+\frac{\epsilon^i{}_{jk}}{f_\pi}\,\langle B|\frac{\tau^k}{2}|A\rangle\,\overline{u}_f\Gamma^\mu_{V\pi}(q,k_\pi)\,u_i.\tag{37}$$

Here, $P^\mu_V(q,k_\pi)$ is defined in Eq. (14), $\Gamma^\mu_{V\pi}(q,k_\pi)$ is defined in Eq. (12), and $\nu \geqslant 1$.

For the axial-vector current, diagram (e) does not contribute, and we find

$$\begin{aligned}\langle A^{i\mu}\rangle_\pi &= \frac{\epsilon^i{}_{jk}}{f_\pi}\,\langle B|\frac{\tau^k}{2}|A\rangle\,\overline{u}_f\Gamma^\mu_{A\pi}(q,k_\pi)\,u_i+\frac{\epsilon^i{}_{jk}}{f_\pi}\,\langle B|\frac{\tau^k}{2}|A\rangle\,\frac{q^\mu}{q^2-m_\pi^2}\,\overline{u}_f\,\frac{(\not{q}+\not{k}_\pi)}{2}\,u_i\\ &+\frac{\epsilon^i{}_{jk}}{f_\pi}\,\langle B|\frac{\tau^k}{2}|A\rangle\,4\kappa_\pi\,\overline{u}_f\left(\frac{\sigma^{\mu\nu}ik_{\pi\nu}}{2M}+\frac{q^\mu}{q^2-m_\pi^2}\,\frac{\sigma^{\alpha\beta}ik_{\pi\alpha}q_\beta}{2M}\right)u_i\\ &+\frac{\delta^i_j}{f_\pi}\,\delta^A_B\,(-4i\beta_\pi)\frac{1}{M}\left(k^\mu_\pi-\frac{q\cdot k_\pi\,q^\mu}{q^2-m_\pi^2}\right)\overline{u}_f u_i\\ &+\frac{\delta^i_j}{f_\pi}\,\delta^A_B\,\frac{-i\kappa_1}{4}\,\frac{1}{M^2}\,\overline{u}_f\left(q_\nu(p_f+p_i)^{\{\nu}\gamma^{\mu\}}-\frac{q\cdot(p_f+p_i)\,q^\mu}{q^2-m_\pi^2}(\not{q}+\not{k}_\pi)\right)u_i.\end{aligned}\tag{38}$$

Here, $\Gamma^\mu_{A\pi}(q,k_\pi)$ is given in Eq. (6). The terms in the first row lead to $\nu \geqslant 1$ contributions. The contributions due to κ_π, β_π, and κ_1 are at $\nu = 2$. We use values fitted in [53] for these couplings. In the last row, $A^{\{\mu}B^{\nu\}} = A^\mu B^\nu + A^\nu B^\mu$.

For the baryon current, diagrams (e) and (f) do not contribute: $\langle J^\mu_B\rangle_\pi = 0$.

For the NC photon production matrix element we find

$$\begin{aligned}\left\langle J^\mu_{NC}\right\rangle_\gamma &= \delta^A_B\,\frac{-iec_1}{M^2}\,\epsilon^{\mu\nu\alpha\beta}\,\overline{u}_f\gamma_\nu k_\alpha\epsilon^*_\beta(k)u_i\\ &+\delta^A_B\,\frac{-iec_1q^\mu}{M^2\left(q^2-m_\pi^2\right)}\,\epsilon^{\lambda\nu\alpha\beta}\,\overline{u}_f\gamma_\lambda q_\nu k_\alpha\epsilon^*_\beta(k)u_i\\ &+\left(\frac{\tau^0}{2}\right)^A_B\,\frac{-iee_1}{2M^2}\,\epsilon^{\mu\nu\alpha\beta}\,\overline{u}_f\gamma_\nu k_\alpha\epsilon^*_\beta(k)u_i\\ &+\left(\frac{\tau^0}{2}\right)^A_B\,\frac{-iee_1q^\mu}{2M^2\left(q^2-m_\pi^2\right)}\,\epsilon^{\lambda\nu\alpha\beta}\,\overline{u}_f\gamma_\lambda q_\nu k_\alpha\epsilon^*_\beta(k)u_i.\end{aligned}$$

Here $\nu = 3$; for $\nu < 3$, there are no contact vertices contributing in this channel. By power counting, we expect that, at low energy, these terms can be neglected compared to the $\nu = 1$ terms. However, according to Ref. [42], these terms may play an important role in coherent photon production. Meanwhile, it

is claimed in Ref. [42] that the origin of these contact vertices is the anomalous interactions of the ω and ρ. But they can also be induced by the off-shell terms in the Δ Lagrangian. Moreover, we can construct meson-dominance terms by using the interaction terms in the last row of Eq. (3) and photon-meson coupling in Eq. (2), which leads to different off-shell behavior of the vertex compared to that of the anomaly term.

V. RESULTS

In this section, after introducing the kinematics, we discuss our results for CC and NC pion production, and also NC photon production, and compare them with available data whenever possible.

A. Kinematics

Figure 2 shows the configuration in the isobaric frame, i.e., the center-of-mass frame of the final nucleon and pion. The momenta are measured in this frame, except those labeled as p^L, which are measured in the laboratory frame with the initial nucleon being static. Detailed analysis of the kinematics is given in Appendix E. The expression for the total cross section is

$$\sigma = \int \frac{\overline{|M|^2}}{32M_n}\frac{1}{(2\pi)^5}\frac{|\vec{p}_\pi|}{E_\pi + E_{nf}}\frac{|\vec{p}^{\,L}_{lf}|}{|\vec{p}^{\,L}_{li}|}\,d\Omega_\pi dE^L_{lf}d\Omega^L_{lf}$$
$$= \int \frac{\overline{|M|^2}}{64M_n^2}\frac{1}{(2\pi)^5}\frac{|\vec{p}_\pi|}{E_\pi + E_{nf}}\frac{\pi}{|\vec{p}^{\,L}_{li}|E^L_{li}}\,d\Omega_\pi dM^2_{\pi n}dQ^2. \tag{39}$$

where $\overline{|M|^2}$ is the average of the total interaction amplitude squared. Based on the equations in Appendix E, we can make the following estimates. For CC pion production, when $E^L_\nu = 0.4\,(0.5)$ GeV, $(M_{\pi n})_{\max} \approxeq 1.17\,(1.24)$ GeV and $Q^2_{\max} \approxeq 0.2\,(0.3)$ GeV^2. We can see that above $E^L_\nu = 0.4$ GeV, the interaction begins to be dominated by the Δ resonance. However, when $E^L_\nu = 0.75$ GeV, $(M_{\pi n})_{\max} \approxeq 1.4$ GeV, and higher resonances, for example $P_{11}(1440)$, may play a role. The exception is $\nu_\mu + p \longrightarrow \mu^- + p + \pi^+$: only $I = 3/2$ can contribute, and the next resonance in this channel is the $\Delta(1600)$, which is accessible only when $E^L_\nu \geqslant 1.8$ GeV. For NC pion production and photon production ($E^L_\gamma \geqslant 0.2$ GeV), when $E^L_\nu = 0.3\,(0.5)$ GeV, $(M_{\pi n})_{\max} \approxeq 1.2\,(1.35)$ GeV and $Q^2_{\max} \approxeq 0.1\,(0.3)$ GeV^2. Here, above $E^L_\nu = 0.3$ GeV, the interaction begins to be dominated by the Δ. However, when $E^L_\nu = 0.6$ GeV, $(M_{\pi n})_{\max} \approxeq 1.4$ GeV, and higher resonances may play a role.

From this analysis, we expect our EFT to be valid at $E^L_\nu \leqslant 0.5$ GeV, since only the Δ resonance can be excited, and $Q^2 \leqslant 0.3$ GeV^2 where meson dominance works for various current form factors [20]. To go beyond this energy regime when we show our results, we require $M_{\pi n} \leqslant 1.4$ GeV and use phenomenological form factors that work when $Q^2 \geqslant 0.3$ GeV^2.

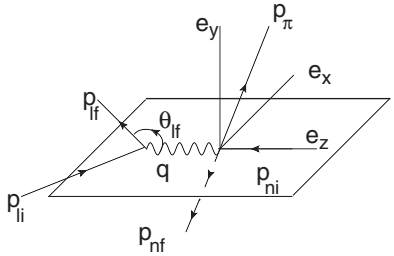

FIG. 2. The configuration in the isobaric frame.

B. CC pion production

In this section, we compare calculated cross sections of CC pion production with ANL [31] and BNL [32] measurements. In both experiments, the targets are hydrogen and deuterium. [All the other experiments use much heavier nuclear targets in (anti)neutrino scattering, and to explain this, we must examine many-body effects.] The beam is composed of muon neutrinos, the average energy of which is 1 and 1.6 GeV for ANL and BNL, respectively. In the ANL data, there is a cut on the invariant mass of the pion and final nucleon system: $M_{\pi n} \leqslant 1.4$ GeV; no such cut is applied in the BNL data. Based on the previous phase-space analysis, this cut clearly reduces the number of events when E_ν is above ~ 0.5 GeV. This can be seen by comparing the two data sets in three different channels shown in Figs. 3 and 4: the ANL data lie systemically below the BNL data. Since the data stretch above 0.5 GeV, in Figs. 3 and 4, we show the "CFF" results (using the conventional form factor in [33]) and the "HFF" results [using the form factor in [26] with the reduced $C^A_5(0)$], with the $M_{\pi n}$ constraint applied. In these calculations, F^{md}, G^{md}, c_Δ, and d_Δ are substituted by the form factors in the literature. The results of our framework, i.e., using the meson-dominance form factor born out of the

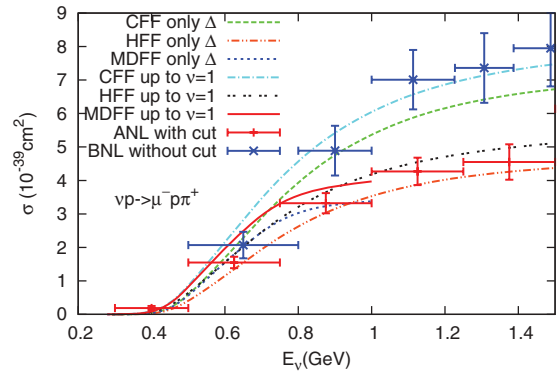

FIG. 3. (Color online) Total cross section for $\nu_\mu + p \longrightarrow \mu^- + p + \pi^+$. "Only Δ" indicates that only diagrams with Δ (both s and u channels) are included. The "up to $\nu = 1$" category includes all the diagrams at leading order. The CFF calculations are done with one of the conventional form factors [33]. The HFF calculations make use of form factor used in [26] with the reduced $C^A_5(0)$. The MDFF calculations are based on the EFT Lagrangian with meson dominance. In the ANL data, $M_{\pi n} \leqslant 1.4$ GeV is applied, while no such cut is applied in the BNL data. For all calculations, $M_{\pi n} \leqslant 1.4$ GeV is applied.

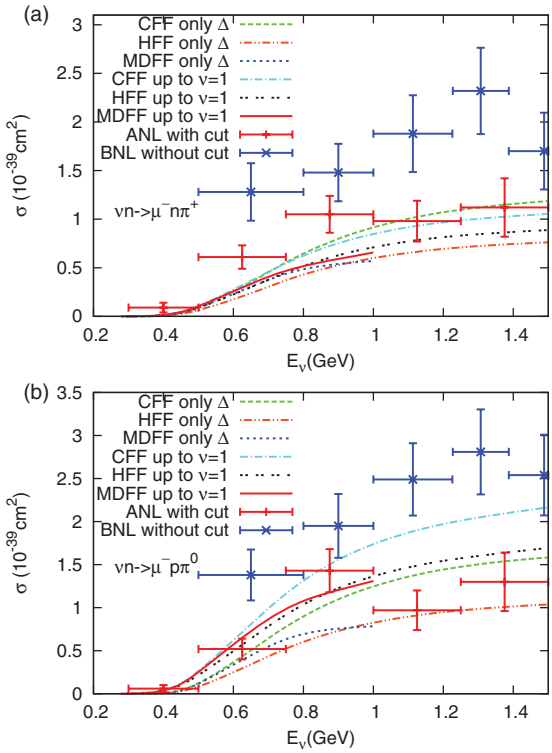

FIG. 4. (Color online) Total cross section for (a) $\nu_\mu + n \longrightarrow \mu^- + n + \pi^+$ and (b) $\nu_\mu + n \longrightarrow \mu^- + p + \pi^0$. In the ANL data, $M_{\pi n} \leqslant 1.4$ GeV is applied, while no such cut is applied in the BNL data. The curves are defined as in Fig. 3.

Lagrangian, are shown as "MDFF" calculations, and these are extrapolated beyond 0.5-GeV limit also. The extrapolations of both CFF and MDFF calculations enable us first to compare our result with similar calculations in [26],[4] and second to see how meson-dominance form factors fail at higher energy. By comparing CFF with MDFF calculations, we can see in the MDFF calculation that the meson-dominance form factors are inadequate for reproducing the conventional form factors above $E_\nu = 0.5$ GeV (although it seems that MDFF results are closer to the data). Hence in the following Fig. 5, we only show the MDFF results with $E_\nu \leqslant 0.5$–0.6 GeV, for which $M_{\pi n} \leqslant 1.4$ GeV holds automatically. Since we believe the EFT is applicable in this low-energy regime, in these plots, we show results including Feynman diagrams up to order $\nu = 1$ and $\nu = 2$.

In Fig. 3, we show the data and calculations for $\nu_\mu + p \longrightarrow \mu^- + p + \pi^+$. As mentioned above, in the "CFF only Δ" calculation, we make use of one set of conventional form factors and include the Feynman diagrams with the Δ in both s and u channels. In the "CFF up to $\nu = 1$" calculation, we use the same form factors and include all the Feynman diagrams up to leading order. These two calculations are quite similar to those done in Ref. [26] *without* reducing C_5^A. Indeed, our results are consistent with theirs. (In Ref. [26], only the s-channel contribution is included in the calculation with "only Δ.") Next, we show two different HFF calculations: one with only Δ (in the s and u channels) and the other with all the diagrams up to $\nu = 1$. Finally, we also show two MDFF calculations up to different order, so that we can compare the MDFF approach with the CFF approach.

First, we can see that both CFF and MDFF calculations with only Δ diagrams are consistent with the data at $E_\nu \leqslant 0.5$ GeV. Introducing other diagrams up to order $\nu = 1$ is still allowed by the data at low energy, although they indeed increase the cross section noticeably. Second, in Ref. [26], a reduced $C_5^A(0)$ is introduced, primarily to reduce the calculated cross sections above $E_\nu = 1$ GeV, which can be seen by comparing CFF calculations with HFF calculations. However, since we are only concerned with the $E_\nu \leqslant 0.5$ GeV region, in which we see satisfactory agreement between our calculations and the data, we will keep the $C_5^A(0)$ fitted from the Δ's free width. Furthermore, in the original spectrum-averaged $d\sigma/dQ^2$ data of ANL [31], the contributions from $E_\nu \leqslant 0.5$ GeV neutrinos are excluded, so comparing calculations with data at low energy is not feasible at this stage, and we will not show our $d\sigma/dQ^2$ here.

In Fig. 4, we show the data and calculations for $\nu_\mu + n \longrightarrow \mu^- + n + \pi^+$ and $\nu_\mu + n \longrightarrow \mu^- + p + \pi^0$. We can see that the situations in these two processes are quite similar to that in Fig. 3: the results of the CFF and MDFF approaches are consistent with the data at low energy. Again the differences between the two approaches with the same diagrams begin to show up when the neutrino energy goes beyond 0.5 GeV. Although the pion production is still dominated by the Δ, if we compare cross sections (from the same calculation) in Figs. 3 and 4, we see that other diagrams introduce significant contributions and violate the naive estimate of the ratio of the three channels' cross sections based on isospin symmetry and Δ dominance. Moreover, the reduction of C_5^A significantly reduces the cross section in these two channels if we compare the two HFF calculations with the corresponding CFF calculations.

In Fig. 5, we begin to investigate the convergence of our calculations in different channels in neutrino and antineutrino scattering. We show the MDFF calculations based on our EFT Lagrangian up to different orders. We see that the power counting makes sense systematically in different channels: including N intermediate state and contact terms up to $\nu = 1$ changes the "only Δ" calculation non-negligibly. Far below resonance, the Δ contribution is less important compared to that in other diagrams, and it begins to dominate around 0.4 GeV. This is consistent with the power counting discussed in Sec. IV. Moreover, the $\nu = 2$ terms do not change the "up to $\nu = 1$" results significantly. All the calculations of neutrino scattering are consistent with the limited data from ANL. We can see that the cross section for antineutrino scattering is generally smaller than that of neutrino scattering, due to the relative sign chosen between $V^{i\mu}$ and $A^{i\mu}$ in the Feynman diagrams having Δ. The sign between $V^{i\mu}$ and $A^{i\mu}$ in other diagrams is well defined in our Lagrangian. The relative sign between Δ's contribution and all the rest diagrams' contributions is also well determined by the relation between

[4]The calculation in [26] without reduction of $C_5^A(0)$ should be close to the CFF calculation [33], although the details of the form factors are different.

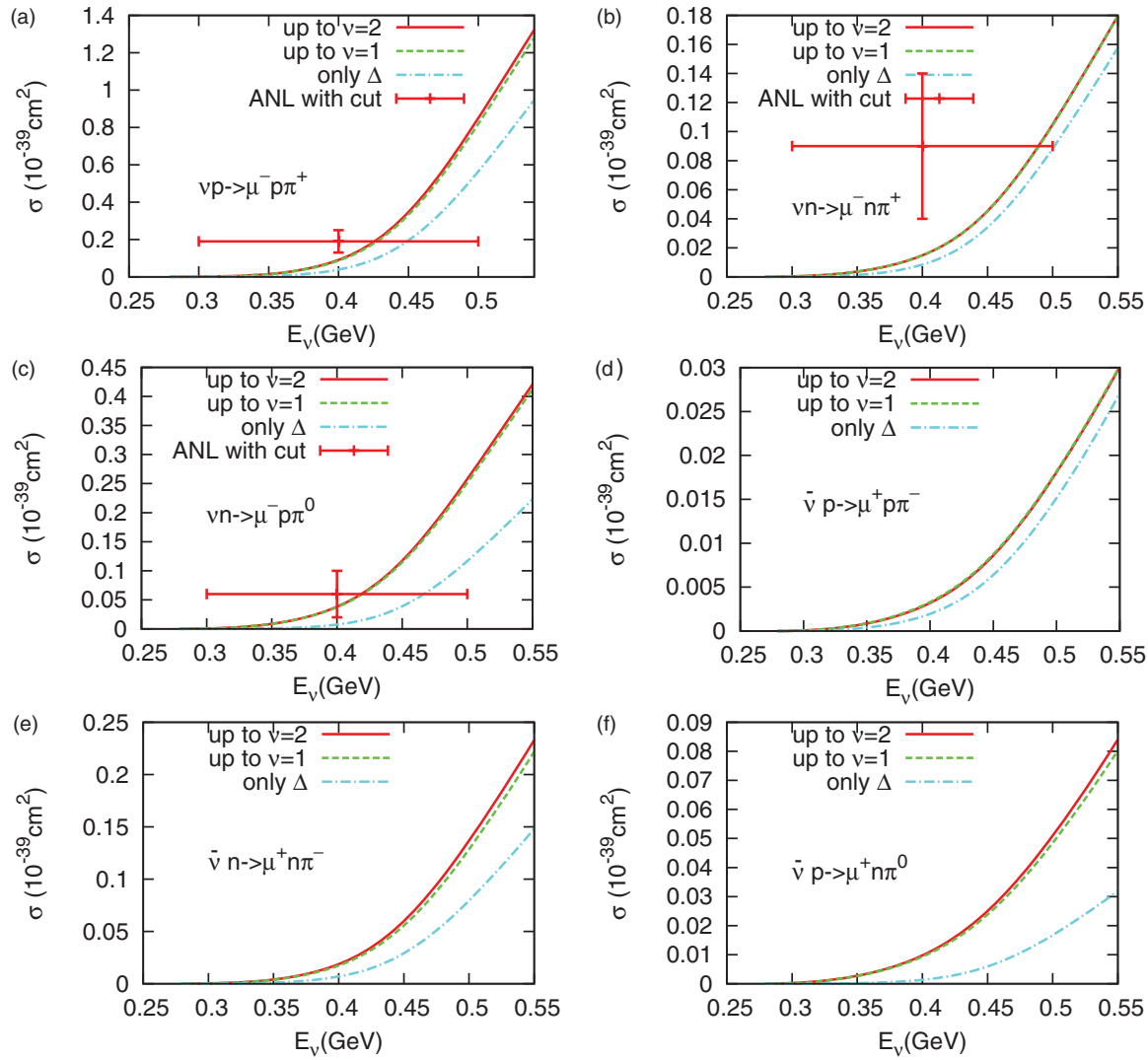

FIG. 5. (Color online) Total cross section for CC pion production due to neutrino and antineutrino scattering off nucleons. Here "only Δ" indicates that only diagrams with Δ (both s and u channels) are included, "up to $\nu = 1$" includes all the diagrams at leading order, and "up to $\nu = 2$" includes higher-order contact terms, whose couplings are from Ref. [53]. In the ANL data, $M_{\pi n} \leqslant 1.4$ GeV. For calculations, $M_{\pi n} \leqslant 1.4$ GeV is applied.

h_A and C_5^A in Eq. (29), although it has been investigated phenomenologically in Ref. [26].

C. NC pion production

In this section, we discuss the results for NC pion production in (anti)neutrino scattering. In Fig. 6, the results in the MDFF approach are shown for calculations including diagrams of different orders. The channels are explained in each plot. Since all of the available data for NC pion production are spectrum-averaged, and neutrinos with $E_\nu \leqslant 0.5$ GeV have a small weight in such analyses, we do not compare our results with data. Here we focus on the convergence of our calculations; introducing the $\nu = 2$ terms does not change the total cross section significantly. However, we also see the violation of isospin symmetry in the "up to $\nu = 1$" and "up to $\nu = 2$" calculations in each plot, if we compare each pair of channels in Fig. 6. In principle, if there is no baryon current contribution in NC production, we should see that the two channels in each plot yield the same results. For example, isospin symmetry implies $\langle p, \pi^0 | V^{0\mu}, A^{0\mu} | p \rangle = \langle n, \pi^0 | V^{0\mu}, A^{0\mu} | n \rangle$ and $\langle p, \pi^0 | J_B^\mu | p \rangle = -\langle n, \pi^0 | J_B^\mu | n \rangle$. So with "only Δ," we cannot see the difference between the two cross sections, since the (isoscalar) baryon current cannot induce transitions from N to Δ. After introducing nonresonant diagrams, we would expect them to be different, as confirmed in the first plot in Fig. 6 for example. This analysis can be applied to other channels, and we clearly see the nonresonant contributions.

D. NC photon production

In this section we focus on NC photon production. The results are shown in Fig. 7. Besides NC π^0 production,

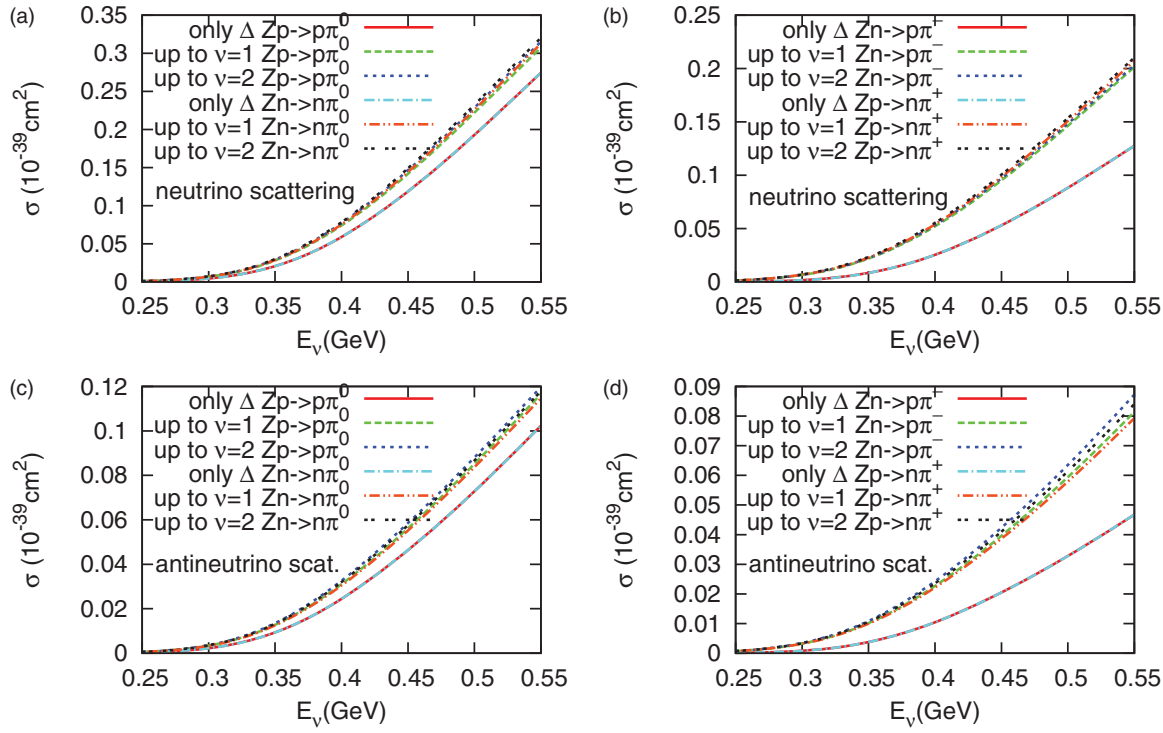

FIG. 6. (Color online) Total cross section for NC π production due to neutrino and antineutrino scattering off nucleons. The curves are defined as in Fig. 5, and the channels are also indicated.

this process is another important background in neutrino experiments. One important difference between NC photon production and CC and NC pion production is that all of the $\nu = 2$ terms do not contribute in this process. Therefore, we include the two $\nu = 3$ terms in NC photon production, namely the e_1 and c_1 couplings in Eq. (39), besides terms due to the form factors. Moreover, these two couplings are singled out in Ref. [42] as the low-energy manifestations of anomalous interactions involving ρ and ω, and they are believed to give important contributions in coherent photon production from nuclei. Here we also investigate the consequences of these two couplings. We emphasize that, from the EFT perspective, the only way to determine these two couplings is by comparing the final theoretical result with data, rather than by calculating them from anomalous interactions, which are not necessarily the only high-energy physics contributing to these two operators. For example, as we discussed before, an off-shell coupling between N, π, and Δ can introduce the same matrix element as the c_1 term. Changing the off-shell couplings would also change the contact term to make the theory independent of the choice of off-shell couplings. Nevertheless, to perform concrete calculations without precise information on the coupling strengths, we use the values from Ref. [42] ($c_1 = 1.5, e_1 = 0.8$).

We can see the convergence of our calculations in Fig. 7. The two couplings introduced in the "up to $\nu = 3$" calculations increase the total cross section in both channels for both neutrino and antineutrino scattering, although the change is quite small. This constructive behavior is consistent with the results in Ref. [42].

Naive power counting, however, does not give an accurate comparison between the Δ contributions and the N contributions at very low energy. First, the neutron does not have an electric charge, so its current should appear at higher order than the naive estimate would indicate. Second, for the proton, due to the cancellation between the baryon current and the vector current, the neutral current is mainly composed of the axial-vector current, which reduces the strength of the neutral current. Because of these two effects, the contributions of Compton-like diagrams are smaller than the power counting indicates.

VI. SUMMARY

Neutrinoproduction of photons and pions from nucleons and nuclei produce important backgrounds in neutrino-oscillation experiments and therefore must be understood quantitatively. In this work, we studied the productions from free nucleons in a Lorentz-covariant, chirally invariant, meson-baryon EFT. For (anti)neutrino energy around 0.5 GeV, the Δ resonance is important. We therefore included the Δ degrees of freedom explicitly in our EFT Lagrangian, in a manner that is consistent with both Lorentz covariance and chiral symmetry.

It is well known that in a Lagrangian with a finite number of interaction terms, including the Δ as a Rarita-Schwinger field leads to inconsistencies for strong couplings, strong fields, or large field variations. In a modern EFT with an infinite number of interaction terms, however, these pathologies can be removed, if we work at low energies with weak boson

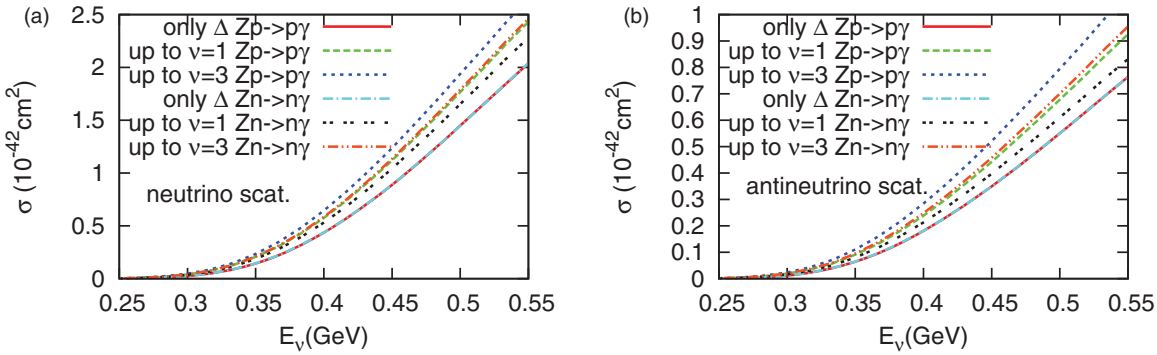

FIG. 7. (Color online) Total cross section for NC photon production due to neutrino and antineutrino scattering off nucleons. Here "only Δ" indicates that only diagrams with Δ (both s and u channels) are included, "up to $\nu = 1$" includes all the diagrams at leading order, and "up to $\nu = 3$" includes higher-order diagrams.

fields. This is clarified in our previous work [23]. Ambiguous and so-called off-shell couplings involving Δ have also been shown to be redundant in the modern EFT framework, because these couplings produce terms that can be absorbed into the contact terms in the EFT Lagrangian. Thus the Δ resonance can be introduced in our EFT Lagrangian in a consistent way.

Because of the symmetries built into our Lagrangian, the vector and baryon currents are conserved and the axial-vector currents are partially conserved automatically, which is not true in some other approaches to this problem (with special constraints among different form factors having to be introduced by hand to conserve vector current in other approaches). Needless to say, the conserved vector and baryon currents are crucial for computing photon production. We discussed in detail how the meson-dominance mechanism works in our matrix element calculations, which is the key ingredient in current conservation. By using vector and axial-vector transition currents that were calibrated in pion production at high energies, we found results for pion production at lower energies ($E_\nu^{\rm Lab} \leqslant 0.5$ GeV) that are consistent with the (limited) data. This is also true when vertices described by meson dominance were used. On the other hand, the couplings introduced to generate meson dominance are relevant in other problems. For example, the interactions in Eq. (18) lead to a proper description of the vector transition current at nonzero Q^2 and meanwhile it is relevant to two-body currents: suppose a photon is absorbed by one nucleon producing a Δ which then interacts with other nucleon through the interactions mentioned above.

Moreover, we studied the convergence of our power-counting scheme at low energies (where the Δ needs to be counted differently in different energy regions) and found that next-to-leading-order tree-level corrections are small. This power-counting scheme is different from the canonical one, because it can be used in nuclear many-body problems. For example, the lowest order in this scheme is the mean-field approximation, if the calculation is done for the property of the nuclear ground states. The discussion on this can be found in [17–19]. It is certainly interesting to see how the power counting that we have for scattering off nucleons works in the scattering off nuclei.

Finally, we computed NC photon production and explored the power counting in this problem. The difference between the NC photon production and pion production is that, at $\nu = 2$, no diagrams contribute in the photon case, while there are several in pion production. So we proceeded to include $\nu = 3$ diagrams induced by two contact interactions, c_1 and e_1 terms. They have been studied in [42], and they are believed to be the low-energy manifestation of anomalous ρ and ω interactions. We pointed out the existence of other sources including off-shell couplings of Δ and possible meson-dominance terms. Nevertheless, by using two coupling strengths calibrated to anomalous ρ and ω interactions [42], we found that, at least for a nucleon target, their contributions are very small, as expected based on power counting.

We are currently using this QHD EFT framework to study the electroweak response of the nuclear many-body system, so that we can extend our results to photon and pion neutrinoproduction from nuclei, which are the true targets in existing neutrino-oscillation experiments.

ACKNOWLEDGMENTS

XZ thanks Mikhail Gorshteyn for the careful reading of the manuscript. This work was supported in part by the Department of Energy under Contract No. DE–FG02–87ER40365.

APPENDIX A: CHIRAL SYMMETRY AND ELECTROWEAK INTERACTIONS IN QHD EFT

Details on chiral symmetry and electroweak interactions in QHD EFT can be found in [23,24]. We introduce background fields including $\mathsf{v}^\mu \equiv \mathsf{v}^{i\mu}\tau_i/2$ (isovector vector), $\mathsf{v}^\mu_{(s)}$ (isoscalar vector), and $\mathsf{a}^\mu \equiv \mathsf{a}^{i\mu}\tau_i/2$ (isovector axial vector), where $i = x, y, z$ or $+1, 0, -1$. They couple to the corresponding currents in QCD. We define $r^\mu = \mathsf{v}^\mu + \mathsf{a}^\mu$ and $l^\mu = \mathsf{v}^\mu - \mathsf{a}^\mu$. Under $\mathrm{SU}(2)_L \otimes \mathrm{SU}(2)_R \otimes \mathrm{U}(1)_B$ symmetry transformations, these fields should change in the following way: $l^\mu \to L\, l^\mu L^\dagger + i L\, \partial^\mu L^\dagger$ $\{L = \exp[-i\theta_{Li}(x)\,\frac{\tau^i}{2}]\}$, $r^\mu \to R\, r^\mu R^\dagger + i R\, \partial^\mu R^\dagger$ $\{R = \exp[-i\theta_{Ri}(x)\,\frac{\tau^i}{2}]\}$, and $\mathsf{v}^\mu_{(s)} \to \mathsf{v}^\mu_{(s)} - \partial^\mu\theta$. Here, $\theta_{Li}(x)$, $\theta_{Ri}(x)$, and $\theta(x)$ are the rotation angles. We

can construct field strength tensors $f_{L\mu\nu} \equiv \partial_\mu l_\nu - \partial_\nu l_\mu - i[l_\mu, l_\nu] \to L f_{L\mu\nu} L^\dagger$, and $f_{R\mu\nu}$ and $f_{s\mu\nu}$ are constructed in the same way.

Now we discuss nonlinear transformations of dynamical degrees freedom in our model:

$$U \equiv \exp\left[2i\frac{\pi_i(x)}{f_\pi}t^i\right] \to L U R^\dagger, \tag{A1}$$

$$\xi \equiv \sqrt{U} = \exp\left[i\frac{\pi_i}{f_\pi}t^i\right] \to L\xi h^\dagger = h\,\xi R^\dagger, \tag{A2}$$

$$\begin{aligned}\widetilde{v}_\mu &\equiv \frac{-i}{2}[\xi^\dagger(\partial_\mu - i l_\mu)\xi + \xi(\partial_\mu - i r_\mu)\xi^\dagger] \equiv \widetilde{v}_{i\mu}t^i \\ &\to h\,\widetilde{v}_\mu h^\dagger - ih\,\partial_\mu h^\dagger,\end{aligned} \tag{A3}$$

$$\begin{aligned}\widetilde{a}_\mu &\equiv \frac{-i}{2}[\xi^\dagger(\partial_\mu - i l_\mu)\xi - \xi(\partial_\mu - i r_\mu)\xi^\dagger] \equiv \widetilde{a}_{i\mu}t^i \\ &\to h\,\widetilde{a}_\mu h^\dagger,\end{aligned} \tag{A4}$$

$$\widetilde{\partial}_\mu U \equiv \partial_\mu U - i l_\mu U + i U r_\mu \to L\,\widetilde{\partial}_\mu U\, R^\dagger, \tag{A5}$$

$$\begin{aligned}(\widetilde{\partial}_\mu\psi)_\alpha &\equiv (\partial_\mu + i\,\widetilde{v}_\mu - i\mathsf{v}_{(s)\mu}B)_\alpha^{\ \beta}\psi_\beta \\ &\to \exp[-i\theta(x)B]\,h_\alpha^{\ \beta}(\widetilde{\partial}_\mu\psi)_\beta,\end{aligned} \tag{A6}$$

$$\widetilde{v}_{\mu\nu} \equiv -i[\widetilde{a}_\mu, \widetilde{a}_\nu] \to h\,\widetilde{v}_{\mu\nu}h^\dagger, \tag{A7}$$

$$F^{(\pm)}_{\mu\nu} \equiv \xi^\dagger f_{L\mu\nu}\,\xi \pm \xi f_{R\mu\nu}\,\xi^\dagger \to h F^{(\pm)}_{\mu\nu} h^\dagger, \tag{A8}$$

$$\widetilde{\partial}_\lambda F^{(\pm)}_{\mu\nu} \equiv \partial_\lambda F^{(\pm)}_{\mu\nu} + i[\widetilde{v}_\lambda,\ F^{(\pm)}_{\mu\nu}] \to h\,\widetilde{\partial}_\lambda F^{(\pm)}_{\mu\nu} h^\dagger. \tag{A9}$$

In the preceding equations, t^i are the generators of reducible representations of SU(2). The $f_\pi \approx 93$ MeV is the pion-decay constant. We generically label non-Goldstone isospin multiplets including the nucleon, ρ meson, and Δ by $\psi_\alpha = (N_A, \rho_i, \Delta_a)_\alpha$. B is the baryon number of the particle. The transformations of the isospin and chiral singlets V_μ and ϕ are trivial. The dual field tensors are defined as $\overline{F}^{(\pm)\mu\nu} \equiv \epsilon^{\mu\nu\alpha\beta}F^{(\pm)}_{\alpha\beta}$, which have the same chiral transformations as the ordinary field tensors. The objects shown here are the building blocks for constructing the Lagrangian.

Electroweak interactions of quarks in the Standard Model [23,24,54,55] determine the form of the background fields in terms of the vector bosons $W^\pm_\mu$, Z_μ, and A_μ:

$$\begin{aligned}l_\mu &= -e\frac{\tau^0}{2}A_\mu + \frac{g}{\cos\theta_w}\sin^2\theta_w\frac{\tau^0}{2}Z_\mu - \frac{g}{\cos\theta_w}\frac{\tau^0}{2}Z_\mu \\ &\quad - g V_{ud}\left(W^{+1}_\mu\frac{\tau_{+1}}{2} + W^{-1}_\mu\frac{\tau_{-1}}{2}\right),\end{aligned} \tag{A10}$$

$$r_\mu = -e\frac{\tau^0}{2}A_\mu + \frac{g}{\cos\theta_w}\sin^2\theta_w\frac{\tau^0}{2}Z_\mu, \tag{A11}$$

$$\mathsf{v}_{(s)\mu} = -e\frac{1}{2}A_\mu + \frac{g}{\cos\theta_w}\sin^2\theta_w\frac{1}{2}Z_\mu, \tag{A12}$$

where g is the SU(2) charge, θ_w is the weak mixing angle, and V_{ud} is the CKM matrix element corresponding to u and d quark mixing.

If we define the interactions with background fields as

$$\begin{aligned}\mathcal{L}_{\rm ext} &\equiv \mathsf{v}_{i\mu}V^{i\mu} - \mathsf{a}_{i\mu}A^{i\mu} + \mathsf{v}_{(s)\mu}J^{B\mu} \\ &= J^L_{i\mu}\,l^{i\mu} + J^R_{i\mu}\,r^{i\mu} + \mathsf{v}_{(s)\mu}J^{B\mu},\end{aligned} \tag{A13}$$

define electroweak interactions as

$$\begin{aligned}\mathcal{L}_I &= -eJ^{EM}_\mu A^\mu - \frac{g}{\cos\theta_w}J^{NC}_\mu Z^\mu \\ &\quad - g V_{ud}\,J^L_{+1\mu}W^{+1\mu} - g V_{ud}\,J^L_{-1\mu}W^{-1\mu},\end{aligned} \tag{A14}$$

and use Eqs. (A10) to (A12), we can see that

$$J^L_{i\mu} \equiv \tfrac{1}{2}(V_{i\mu} + A_{i\mu}), \tag{A15}$$

$$J^R_{i\mu} \equiv \tfrac{1}{2}(V_{i\mu} - A_{i\mu}), \tag{A16}$$

$$J^{EM}_\mu = V^0_\mu + \tfrac{1}{2}J^B_\mu, \tag{A17}$$

$$J^{NC}_\mu = J^{L0}_\mu - \sin^2\theta_w\,J^{EM}_\mu. \tag{A18}$$

Here, J^B_μ is the baryon current, defined to be coupled to $\mathsf{v}^\mu_{(s)}$. These relations are consistent with the charge algebra $Q = T^0 + B/2$ (where B is the baryon number). $V^{i\mu}$ and $A^{i\mu}$ are the isovector vector current and the isovector axial-vector current, respectively. We do not discuss "seagull" terms of higher order in the couplings, i.e. two photons in one vertex, because they do not enter in our calculations [10,24].

APPENDIX B: FORM FACTORS FOR CURRENTS

Here we use matrix elements of the various currents to define the form factors produced by the Lagrangian [5]. By using information presented in Appendix. A and the Lagrangian in Sec. II, we can determine the matrix elements:

$$\begin{aligned}\langle N,B|V^i_\mu|N,A\rangle &= \left[\overline{u}_f\gamma_\mu u_i + \frac{\beta^{(1)}}{M^2}\overline{u}_f(q^2\gamma_\mu - \not{q}q_\mu)u_i - \frac{g_\rho}{g_\gamma}\frac{q^2g_{\mu\nu}-q_\mu q_\nu}{q^2-m_\rho^2}\overline{u}_f\gamma^\nu u_i\right]\langle B|\frac{\tau^i}{2}|A\rangle \\ &\quad + \left[2\lambda^{(1)}\overline{u}_f\frac{\sigma_{\mu\nu}iq^\nu}{2M}u_i - \frac{f_\rho g_\rho}{g_\gamma}\frac{q^2}{q^2-m_\rho^2}\overline{u}_f\frac{\sigma_{\mu\nu}iq^\nu}{2M}u_i\right]\langle B|\frac{\tau^i}{2}|A\rangle,\end{aligned} \tag{B1}$$

$$\begin{aligned}\langle N,B|J^B_\mu|N,A\rangle &= \left[\overline{u}_f\gamma_\mu u_i + \frac{\beta^{(0)}}{M^2}\overline{u}_f(q^2\gamma_\mu - \not{q}q_\mu)u_i - \frac{2g_v}{3g_\gamma}\frac{q^2g_{\mu\nu}-q_\mu q_\nu}{q^2-m_v^2}\overline{u}_f\gamma^\nu u_i\right]\delta^A_B \\ &\quad + \left[2\lambda^{(0)}\overline{u}_f\frac{\sigma_{\mu\nu}iq^\nu}{2M}u_i - \frac{2f_vg_v}{3g_\gamma}\frac{q^2}{q^2-m_v^2}\overline{u}_f\frac{\sigma_{\mu\nu}iq^\nu}{2M}u_i\right]\delta^A_B,\end{aligned} \tag{B2}$$

$$\langle N,B;\pi,j,k_\pi|A^i_\mu|N,A\rangle = -\frac{\epsilon^i_{jk}}{f_\pi}\langle B|\frac{\tau^k}{2}|A\rangle\,\overline{u}_f\gamma^\nu u_i\left[g_{\mu\nu}+\frac{\beta^{(1)}}{M^2}(q\cdot(q-k_\pi)g_{\mu\nu}-(q-k_\pi)_\mu q_\nu)\right.$$
$$\left.-\frac{g_\rho}{g_\gamma}\frac{q\cdot(q-k_\pi)g_{\mu\nu}-(q-k_\pi)_\mu q_\nu}{(q-k_\pi)^2-m_\rho^2}\right]$$
$$-\frac{\epsilon^i_{jk}}{f_\pi}\langle B|\frac{\tau^k}{2}|A\rangle\,\overline{u}_f\frac{\sigma_{\mu\nu}iq^\nu}{2M}u_i\left[2\lambda^{(1)}-\frac{f_\rho g_\rho}{g_\gamma}\frac{q\cdot(q-k_\pi)}{(q-k_\pi)^2-m_\rho^2}\right]. \tag{B3}$$

Now we consider $\langle N,B|A^i_\mu|N,A\rangle$ and $\langle N,B;\pi,j|V^i_\mu|N,A\rangle$. In the chiral limit, we find

$$\langle N,B|A^i_\mu|N,A\rangle = -\langle B|\frac{\tau^i}{2}|A\rangle\overline{u}_f\gamma^\nu\gamma^5 u_i\left[g_A\left(g_{\mu\nu}-\frac{q_\mu q_\nu}{q^2}\right)-\frac{\beta^{(1)}_A}{M^2}(q^2g_{\mu\nu}-q_\mu q_\nu)-2c_{a_1}g_{a_1}\frac{q^2g_{\mu\nu}-q_\mu q_\nu}{q^2-m^2_{a_1}}\right], \tag{B4}$$

$$\langle N,B;\pi,j,k_\pi|V^i_\mu|N,A\rangle = \frac{\epsilon^i_{jk}}{f_\pi}\langle B|\frac{\tau^k}{2}|A\rangle\,\overline{u}_f\gamma^\nu\gamma^5 u_i\left[g_Ag_{\mu\nu}-\frac{\beta^{(1)}_A}{M^2}(q\cdot(q-k_\pi)g_{\mu\nu}-(q-k_\pi)_\mu q_\nu)\right.$$
$$\left.-2c_{a_1}g_{a_1}\frac{q\cdot(q-k_\pi)g_{\mu\nu}-(q-k_\pi)_\mu q_\nu}{(q-k_\pi)^2-m^2_{a_1}}\right]. \tag{B5}$$

Suppose that there is only one manifestly chiral-symmetry-breaking term, i.e., the mass term for pions; then the pion-pole contribution associated with the g_A coupling in $\langle N,B|A^i_\mu|N,A\rangle$ will become $g_A[g_{\mu\nu}-q_\mu q_\nu/(q^2-m_\pi^2)]$, while the other parts in $\langle N,B|A^i_\mu|N,A\rangle$, as well as the whole $\langle N,B;\pi,j|V^i_\mu|N,A\rangle$, will remain unchanged. However, we must realize that there are other possible chiral-symmetry-breaking terms contributing to $\langle N,B|A^i_\mu|N,A\rangle$. For example, $(m_\pi^2/M)\,\overline{N}i\gamma^5(U-U^\dagger)N$ can contribute to $\langle N,B|A^i_\mu|N,A\rangle$ as

$$-\frac{2m_\pi^2}{M^2}\frac{q_\mu\,\not{q}\gamma^5}{q^2-m_\pi^2}\langle B|\frac{\tau^i}{2}|A\rangle.$$

To simplify the fitting procedures, we use the following form factors [where G_A^{md} can be found in Eq. (13)]:

$$\langle N,B|A^i_\mu|N,A\rangle = -G_A^{md}(q^2)\langle B|\frac{\tau^i}{2}|A\rangle\overline{u}_f\left(g_{\mu\nu}-\frac{q_\mu q_\nu}{q^2-m_\pi^2}\right)\gamma^\nu\gamma^5 u_i, \tag{B6}$$

$$\langle N,B;\pi,j,k_\pi|V^i_\mu|N,A\rangle = \frac{\epsilon^i_{jk}}{f_\pi}\langle B|\frac{\tau^k}{2}|A\rangle\,\overline{u}_f\gamma^\nu\gamma^5 u_i\left[g_Ag_{\mu\nu}+\delta G_A^{md}[(q-k_\pi)^2]\frac{q\cdot(q-k_\pi)g_{\mu\nu}-(q-k_\pi)_\mu q_\nu}{(q-k_\pi)^2}\right]. \tag{B7}$$

Finally, we calculate the pion form factor $\langle\pi,k|V^i_\mu|\pi,j\rangle$:

$$\langle\pi,k,k_\pi|V^i_\mu|\pi,j,k_\pi-q\rangle = i\epsilon^{ij}_{\ \ k}(2k_\pi-q)_\mu+2i\frac{g_{\rho\pi\pi}}{g_\gamma}\epsilon^{ij}_{\ \ k}\frac{q^2}{m_\rho^2}\frac{1}{q^2-m_\rho^2}(q\cdot k_\pi q_\mu-q^2k_{\pi\mu}),$$
$$q^2\to m_\rho^2 \text{ in numerator} \longrightarrow i\epsilon^{ij}_{\ \ k}(2k_\pi-q)_\mu+2i\frac{g_{\rho\pi\pi}}{g_\gamma}\epsilon^{ij}_{\ \ k}\frac{1}{q^2-m_\rho^2}(q\cdot k_\pi q_\mu-q^2k_{\pi\mu}). \tag{B8}$$

APPENDIX C: POWER COUNTING FOR DIAGRAMS WITH Δ

Including Δ resonances in calculations, we have a new mass scale $\delta\equiv m-M\approx 300$ MeV. We must also consider the order of the Δ width Γ. Formally, it is counted as $O(Q^3/M^2)$; however, numerical calculations with Eq. (D2) indicate that it should be counted as $O(Q^3\times 10/M^2)$. Because of these two issues, we have to rethink the power counting of diagrams involving δ in two energy regimes. One is near the resonance, while the other is at lower energies, away from the resonance. In the resonance region, the Δ propagator scales like

$$S_F\sim\frac{1}{i\Gamma}+O\left(\frac{1}{M}\right)\approx\frac{1}{10i\;O(Q^3/M^2)}\approx\frac{1}{i\;O(Q^2/M)}$$
$$\sim\frac{1}{O(Q)}\frac{M}{i\;O(Q)}, \tag{C1}$$

where the $O(1/M)$ comes from nonpole terms. In the lower-energy region,

$$S_F\sim\frac{1}{2[\delta-O(Q)]-10i\;O(Q^3/M^2)}+O\left(\frac{1}{M}\right)$$
$$\sim\frac{1}{O(Q)}\frac{O(Q)}{2\delta}+O\left(\frac{1}{M}\right)\approx\frac{1}{O(Q)}\frac{O(Q)}{M}. \tag{C2}$$

So compared to the normal power counting mentioned above, in which the nucleon propagator scales as $1/O(Q)$, for diagrams involving one Δ in the s channel, we take $\nu\to\nu-1$ in the resonance regime and $\nu\to\nu+1$ away from the resonance.

APPENDIX D: RENORMALIZED Δ PROPAGATOR

In this work, Δ's propagator [47] is dressed as

$$\begin{aligned} S_F^{\mu\nu}(p) \equiv & -\frac{\not{p}+m}{p^2-m^2-\Pi(p^2)+im\Gamma(p^2)}P^{(\frac{3}{2})\mu\nu} \\ & -\frac{1}{\sqrt{3}m}P_{12}^{(\frac{1}{2})\mu\nu}-\frac{1}{\sqrt{3}m}P_{21}^{(\frac{1}{2})\mu\nu} \\ & +\frac{2}{3m^2}(\not{p}+m)P_{22}^{(\frac{1}{2})\mu\nu} \\ & +O(\Gamma/m)\times\text{nonpole terms}, \end{aligned} \tag{D1}$$

$$\begin{aligned} \Gamma(p^2) = & \frac{\pi}{12mp^4}\frac{h_A^2}{(4\pi f_\pi)^2}(p^2+M^2+2Mm) \\ & \times[(p^2-M^2)^2-(p^2+3M^2)m_\pi^2] \\ & \times\sqrt{(p^2-M^2)^2-4p^2m_\pi^2}. \end{aligned} \tag{D2}$$

Here,

$$P^{(\frac{3}{2})\mu\nu} = g^{\mu\nu}-\frac{1}{3}\gamma^\mu\gamma^\nu+\frac{1}{3p^2}\gamma^{[\mu}p^{\nu]}\not{p}-\frac{2}{3p^2}p^\mu p^\nu, \tag{D3}$$

$$P_{11}^{(\frac{1}{2})\mu\nu} = \frac{1}{3}\gamma^\mu\gamma^\nu-\frac{1}{3p^2}\gamma^{[\mu}p^{\nu]}\not{p}-\frac{1}{3p^2}p^\mu p^\nu, \tag{D4}$$

$$P_{12}^{(\frac{1}{2})\mu\nu} = \frac{1}{\sqrt{3}p^2}(-p^\mu p^\nu+\gamma^\mu p^\nu\not{p}), \tag{D5}$$

$$P_{21}^{(\frac{1}{2})\mu\nu} = -P_{12}^{(\frac{1}{2})\nu\mu}, \tag{D6}$$

$$P_{22}^{(\frac{1}{2})\mu\nu} = \tfrac{1}{p^2}p^\mu p^\nu. \tag{D7}$$

We take $m = 1232$ MeV as the Breit–Wigner mass [56] and set $\Pi = 0$. Note that Γ is implicitly associated with a factor of $\Theta[p^2-(M+m_\pi)^2]$. And no singularity exists in this propagator at $p^2 = 0$.

APPENDIX E: KINEMATICS

Following a standard calculation, we find the total cross section:

$$\begin{aligned} \sigma &= \int \frac{\overline{|M|^2}}{4|p_{li}^L\cdot p_{ni}^L|}(2\pi)^4\delta^{(4)}\left(\sum_i p_i^L\right)\frac{d^3\vec{p}_{lf}^{\,L}}{(2\pi)^3 2E_{lf}^L}\frac{d^3\vec{p}_\pi^{\,L}}{(2\pi)^3 2E_\pi^L}\frac{d^3\vec{p}_{nf}^{\,L}}{(2\pi)^3 2E_{nf}^L} \\ &= \int \frac{\overline{|M|^2}}{4|p_{li}^L\cdot p_{ni}^L|}(2\pi)^4\delta\left(q^0+p_{ni}^0-p_{nf}^0-p_\pi^0\right)\frac{1}{(2\pi)^3 2E_{nf}}\frac{d^3\vec{p}_{lf}^{\,L}}{(2\pi)^3 2E_{lf}^L}\frac{d^3\vec{p}_\pi}{(2\pi)^3 2E_\pi} \\ &= \int \frac{\overline{|M|^2}}{32M_n}\frac{1}{(2\pi)^5}\frac{|\vec{p}_\pi|}{E_\pi+E_{nf}}\frac{|\vec{p}_{lf}^{\,L}|}{|\vec{p}_{li}^{\,L}|}\,d\Omega_\pi\,dE_{lf}^L\,d\Omega_{lf}^L. \end{aligned} \tag{E1}$$

The variables without an "L" superscript are measured in the isobaric frame (where Δ is static). It is quite complicated to calculate the boundary of phase space in terms of the integration variables in the preceding equations. Later, we will work out the boundary of phase space in terms of the invariant variables Q^2 and $M_{\pi n}$ in the c.m. frame of the whole system, so we would like to have the following:

$$Q^2 = -M_{lf}^2+2E_{li}^L\left(E_{lf}^L-|\vec{p}_{lf}^{\,L}|\cos\theta_{lf}^L\right), \tag{E2}$$

$$M_{\pi n}^2 = \left(q^L+p_{ni}^L\right)^2 = -Q^2+M_n^2+2M_n\left(E_{li}^L-E_{lf}^L\right), \tag{E3}$$

$$dQ^2dM_{\pi n}^2 = 4M_nE_{li}^L\,|\vec{p}_{lf}^{\,L}|dE_{lf}^L\,d\cos\theta_{lf}^L. \tag{E4}$$

By using the invariance of the cross section with respect to rotations around the incoming lepton direction, we have $\int d\Omega_{lf}^L = \int d\cos\theta_{lf}^L\,2\pi$, and thus

$$\sigma = \int \frac{\overline{|M|^2}}{64M_n^2}\frac{1}{(2\pi)^5}\frac{|\vec{p}_\pi|}{E_\pi+E_{nf}}\frac{\pi}{|\vec{p}_{li}^{\,L}|E_{li}^L}\,d\Omega_\pi\,dM_{\pi n}^2\,dQ^2. \tag{E5}$$

In the isobaric frame, there is no constraint on the direction of the outgoing pion due to the kinematics. Thus the boundary of Ω_π is the whole solid angle in the isobaric frame. Now let us work out the boundary of phase space in the c.m. frame. We have

$$\begin{aligned} M_A^2 \equiv p_A^2 &= \left(p_{ni}^L+p_{li}^L\right)^2 = \left(M_n+E_{li}^L\right)^2-\left(E_{li}^L\right)^2 \\ &= M_n^2+2M_nE_{li}^L, \end{aligned} \tag{E6}$$

$$\begin{aligned} M_{\pi n}^2 \equiv (p_\pi+p_{nf})^2 &= \left(p_A^C-p_{lf}^C\right)^2 \\ &= M_A^2+M_{lf}^2-2M_AE_{lf}^C. \end{aligned} \tag{E7}$$

Here, E_{lf}^C is the final lepton's energy in the c.m. frame. From now on, all the quantities in the c.m. frame will be labeled in this way. So, for given E_{li}^L, i.e., M_A, we can see that

$$M_n+M_\pi \leqslant M_{\pi n} \leqslant M_A-M_{lf}. \tag{E8}$$

By using Eq. (E7), we find

$$\left(E_{lf}^C\right)_{\max(\min)} = \frac{M_A^2+M_{lf}^2-\left(M_{\pi n}^2\right)_{\min(\max)}}{2M_A}. \tag{E9}$$

Then, for given E_{li}^L and $M_{\pi n}$ (or E_{lf}^C), using $Q^2 = -M_{lf}^2+2E_{li}^CE_{lf}^C-2E_{li}^C|\vec{p}_{lf}|^C\cos\theta_{lf}^C$ [where θ_{lf}^C is the angle between the outgoing lepton's direction and the incoming lepton's direction in the c.m. frame, and $E_{li}^C = (M_A^2-M_n^2)/2M_A$ is

the initial lepton's energy in the c.m. frame], we finally arrive at

$$\left[Q^2\left(E_{lf}^C\right)\right]_{\min} = -M_{lf}^2 + \frac{2E_{li}^C M_{lf}^2}{E_{lf}^C + \sqrt{\left(E_{lf}^C\right)^2 - M_{lf}^2}}, \tag{E10}$$

$$\left[Q^2\left(E_{lf}^C\right)\right]_{\max} = -M_{lf}^2 + 2E_{li}^C\left(E_{lf}^C + \sqrt{\left(E_{lf}^C\right)^2 - M_{lf}^2}\right). \tag{E11}$$

These equations give a description of the phase-space boundary in terms of the invariants $M_{\pi n}$ and Q^2.

[1] A. A. Aquilar-Arevalo *et al*. (MiniBooNE Collaboration), Phys. Rev. Lett. **100**, 032301 (2008).
[2] T. Katori (for the MicroBooNE Collaboration), AIP Conf. Proc. **1405**, 250 (2011).
[3] B. D. Serot and J. D. Walecka, Adv. Nucl. Phys. **16**, 1 (1986).
[4] B. D. Serot and J. D. Walecka, Int. J. Mod. Phys. E **6**, 515 (1997).
[5] R. J. Furnstahl, B. D. Serot, and H.-B. Tang, Nucl. Phys. A **615**, 441 (1997); **640**, 505(E) (1998).
[6] R. J. Furnstahl and B. D. Serot, Nucl. Phys. A **671**, 447 (2000).
[7] R. J. Furnstahl and B. D. Serot, Nucl. Phys. A **673**, 298 (2000).
[8] R. J. Furnstahl and B. D. Serot, Comments Mod. Phys. **2**, A23 (2000).
[9] B. D. Serot, in *Extended Density Functionals in Nuclear Structure Physics*, Lecture Notes in Physics Vol. 641, edited by G. A. Lalazissis, P. Ring, and D. Vretenar (Springer, Berlin Heidelberg, 2004), p. 31.
[10] B. D. Serot, Ann. Phys. (NY) **322**, 2811 (2007).
[11] M. A. Huertas, Phys. Rev. C **66**, 024318 (2002); **67**, 019901(E) (2003).
[12] M. A. Huertas, Acta Phys. Pol. B **34**, 4269 (2003).
[13] M. A. Huertas, Acta Phys. Pol. B **35**, 837 (2004).
[14] J. McIntire, Acta Phys. Pol. B **35**, 2261 (2004).
[15] J. McIntire, arXiv:nucl-th/0507006.
[16] J. D. Walecka, *Theoretical Nuclear and Subnuclear Physics*, 2nd ed. (World Scientific, Singapore, 2004), Chap. 24.
[17] J. McIntire, Y. Hu, and B. D. Serot, Nucl. Phys. A **794**, 166 (2007).
[18] Y. Hu, J. McIntire, and B. D. Serot, Nucl. Phys. A **794**, 187 (2007).
[19] J. McIntire, Ann. Phys. (NY) **323**, 1460 (2008).
[20] B. D. Serot, Phys. Rev. C **81**, 034305 (2010).
[21] W. Lin and B. D. Serot, Phys. Lett. B **233**, 23 (1989); Nucl. Phys. A **512**, 637 (1990).
[22] W. Lin and B. D. Serot, Nucl. Phys. A **524**, 601 (1991).
[23] B. D. Serot and X. Zhang, in *Advances in Quantum Field Theory*, edited by Sergey Ketov (InTech, Rijeka, Croatia, 2012), Chap. 4.
[24] X. Zhang, Ph.D. thesis, Indiana University, 2012.
[25] J. Gasser and H. Leutwyler, Ann. Phys. (NY) **158**, 142 (1984).
[26] E. Hernández, J. Nieves, and M. Valverde, Phys. Rev. D **76**, 033005 (2007).
[27] G. Ecker, J. Gasser, A. Pich, and E. De Rafael, Nucl. Phys. B **321**, 311 (1989).
[28] G. Ecker, J. Gasser, H. Leutwyler, A. Pich, and E. De Rafael, Phys. Lett. B **223**, 425 (1989).
[29] O. Lalakulich, E. A. Paschos, and G. Piranishvili, Phys. Rev. D **74**, 014009 (2006).
[30] K. M. Graczyk and J. T. Sobczyk, Phys. Rev. D **77**, 053001 (2008).
[31] G. M. Radecky *et al*., Phys. Rev. D **25**, 1161 (1982).
[32] T. Kitagaki *et al*., Phys. Rev. D **34**, 2554 (1986).
[33] K. M. Graczyk, D. Kiełczewska, P. Przewłocki, and J. T. Sobczyk, Phys. Rev. D **80**, 093001 (2009).
[34] C. Praet, O. Lalakulich, N. Jachowicz, and J. Ryckebusch, Phys. Rev. C **79**, 044603 (2009).
[35] S. L. Adler, Ann. Phys. (NY) **50**, 189 (1968).
[36] C. H. Llewellyn-Smith, Phys. Rep. **3**, 261 (1972).
[37] P. A. Schreiner and F. Von Hippel, Phys. Rev. Lett. **30**, 339 (1973).
[38] D. Rein and L. M. Sehgal, Ann. Phys. (NY) **133**, 79 (1981).
[39] L. Alvarez-Ruso, S. K. Singh, and M. J. Vicente Vacas, Phys. Rev. C **59**, 3386 (1999).
[40] T. Sato, D. Uno, and T. S. H. Lee, Phys. Rev. C **67**, 065201 (2003).
[41] O. Lalakulich and E. A. Paschos, Phys. Rev. D **71**, 074003 (2005).
[42] R. J. Hill, Phys. Rev. D **81**, 013008 (2010).
[43] O. Lalakulich, T. Leitner, O. Buss, and U. Mosel, Phys. Rev. D **82**, 093001 (2010).
[44] H. Georgi and A. Manohar, Nucl. Phys. B **234**, 189 (1984).
[45] H. Georgi, Phys. Lett. B **298**, 187 (1993).
[46] S. M. Ananyan, B. D. Serot, and J. D. Walecka, Phys. Rev. C **66**, 055502 (2002).
[47] P. J. Ellis and H.-B. Tang, Phys. Rev. C **57**, 3356 (1998).
[48] R. J. Furnstahl, H.-B. Tang, and B. D. Serot, Phys. Rev. C **52**, 1368 (1995).
[49] R. J. Furnstahl, B. D. Serot, and H.-B. Tang, Nucl. Phys. A **598**, 539 (1996).
[50] J. J. Kelly, Phys. Rev. C **70**, 068202 (2004).
[51] T. Ericson and W. Weise, *Pions and Nuclei* (Clarendon, Oxford, 1988).
[52] V. Pascalutsa, Prog. Part. Nucl. Phys. **61**, 27 (2008).
[53] P. J. Ellis and H.-B. Tang, Phys. Rev. C **56**, 3363 (1997).
[54] C. Itzykson and J.-B. Zuber, *Quantum Field Theory* (McGraw–Hill, New York, 1980), Chap. 12.
[55] J. F. Donoghue, E. Golowich, and B. Holstein, *Dynamics of the Standard Model* (Cambridge University Press, New York, 1992), Chap. 2.
[56] C. Amsler *et al*. (Particle Data Group), Phys. Lett. B **667**, 1 (2008).